Journal for ImmunoTherapy of Cancer

Single-cell RNA sequencing of baseline PBMCs predicts ICI efficacy and irAE severity in patients with NSCLC

Gyeong Dae Kim ,[1] So-I Shin,[1] Pureum Sun,[2] Jeong Eun Lee,[3] Chaeuk Chung,[3] Yea Eun Kang,[3] Da Hyun Kang ,[3] Jihwan Park[1]

To cite: Kim GD, Shin S-I, Sun P, *et al*. Single-cell RNA sequencing of baseline PBMCs predicts ICI efficacy and irAE severity in patients with NSCLC. *Journal for ImmunoTherapy of Cancer* 2025;**13**:e011636. doi:10.1136/jitc-2025-011636

► Additional supplemental material is published online only. To view, please visit the journal online (https://doi.org/10.1136/jitc-2025-011636).

Accepted 29 April 2025

[1]Life Science, Gwangju Institute of Science and Technology, Gwangju, Buk-gu, Korea (the Republic of)
[2]Institute for Medical Sciences, College of Medicine, Chungnam National University, Daejeon, South Korea
[3]Department of Internal Medicine, College of Medicine, Chungnam National University, Daejeon, South Korea

Correspondence to
Professor Jihwan Park; jihwan.park@gist.ac.kr

Professor Da Hyun Kang; ibelieveu113@naver.com

ABSTRACT

Background Immune checkpoint inhibitors (ICIs) have transformed treatment and have provided significant clinical benefits and durable responses for patients with advanced non-small cell lung cancer (NSCLC). However, only a small percentage of patients respond to ICI treatment, and immune-related adverse events (irAEs) leading to treatment discontinuation remain challenging. Despite the recognized need for biomarkers to predict both the efficacy of ICIs and the risk of irAEs, such biomarkers are yet to be clearly identified.

Methods In this study, we performed single-cell RNA sequencing (scRNA-seq) of peripheral blood mononuclear cells (PBMCs) from 33 patients with NSCLC before ICIs treatment. To validate our findings, we reanalyzed public scRNA-seq data, conducted a cytometric bead array (CBA), and supported our findings with T-cell receptor sequencing.

Results While the immune response was more pronounced in patients with a favorable prognosis, the hypoxic pathway was more prominent in patients with primary resistance. Lymphocytes such as CD8 T cells, CD4 T cells, and natural killer cells were primarily involved in these pathways, with *PRF1* and *GZMB* expression showing strong associations with favorable prognosis. In contrast, irAEs were mainly linked to myeloid cells, such as monocytes and macrophages. As irAE severity increased, inflammation and the TNF-NFKB1 pathway were more prominent. Specifically, increased expression of *IL1B*, *CXCL8*, and *CXCL2* in monocytes and *TNF* in macrophages was closely associated with severe irAE through involvement in these pathways.
Notably, the increase of *PRF1* and *GZMB* expression showed a close association with both a favorable prognosis and a reduced severity of irAE, which was validated through CBA analysis. Moreover, the expression of these key markers varied according to prognosis and irAE severity regardless of patient background, such as programmed death-ligand 1 expression levels, tumor histology, or prior treatment regimens.

Conclusions This study identified biological pathways and key biomarkers associated with ICI prognosis and irAE severity using PBMC samples before treatment. These findings provide a foundation for improved therapeutic strategies that enhance clinical outcomes while minimizing ICI treatment-associated risks.

WHAT IS ALREADY KNOWN ON THIS TOPIC

⇒ While immune checkpoint inhibitors (ICIs) have emerged as innovative and broadly used treatments that enhance the host immune response, biomarkers and mechanisms to identify patients with low responsiveness or those at risk of immune-related adverse events (irAEs) remain unclear.

WHAT THIS STUDY ADDS

⇒ Lymphocytes—including $CD8^+$ T cells, CD4 T cells, and natural killer (NK) cells—were primarily associated with favorable responses to ICIs (complete response, CR) and showed the upregulation of immune activation and interferon/cytokine signaling pathways. Notably, PRF1 and GZMB were CR specifically elevated in CD8 T cells and NK cells.

⇒ In contrast, myeloid cells, such as monocytes and macrophages, were predominantly involved in the severity of irAEs, with heightened activation of inflammatory and TNF–NF-κB signaling pathways observed in severe irAEs. Specifically, the expression of CXCL8 and IL1B in monocytes and TNF in macrophages was markedly increased in severe irAEs.

⇒ Interestingly, PRF1 and GZMB, which are closely associated with favorable responses, were also upregulated in mild-to-moderate irAEs associated with a favorable prognosis.

HOW THIS STUDY MIGHT AFFECT RESEARCH, PRACTICE OR POLICY

⇒ This study provided biomarkers that potentially serve as a non-invasive screening tool that can identify appropriate patients who are likely to benefit from ICI therapy before treatment. Incorporating such biomarkers into clinical decision-making could help optimize patient selection and minimize the risk of severe toxicity.

BACKGROUND

Immune checkpoint inhibitors (ICIs) have revolutionized treatment paradigms for patients with advanced non-small cell lung cancer (NSCLC), offering remarkable clinical benefits and durable responses.[1] As ICI use has increased not only in advanced lung cancer but also in the early stages, nearly all

patients with lung cancer now receive this therapy.[2] Unlike conventional treatments targeting tumors directly, ICIs enhance the host immune system ability to recognize and eliminate cancer cells, instead of focusing on the tumor itself as is the case in conventional cancer treatments.[3] This shift has highlighted the growing importance of circulating immune cells in cancer cells.

A hallmark of ICIs is their durable response, attributed to adaptive immune memory.[4] However, such long-lasting response expected when ICIs were first developed was observed in only a very small percentage of patients, and the majority of patients experienced primary or acquired resistance (AR). In patients with lung cancer receiving ICI treatment, primary resistance, defined as resistance to the initial treatment, is reported to be 40%.[5] Even among patients who initially respond to ICI treatment, more than half eventually experience disease progression, which is defined as AR.[6] Various studies have attempted to identify the underlying mechanisms of ICI resistance, and it is assumed that both intrinsic and extrinsic tumor cell factors contribute to ICI resistance.[4 7]

ICIs target the programmed death-1 (PD-1)/programmed death ligand 1 (PD-L1) pathway, which regulates immune response termination and plays an important role in self-tolerance.[8] Blocking this PD-1/PD-L1 pathway with ICIs can disrupt this regulation, promoting autoimmune and inflammatory responses and resulting in various immune-related adverse events (irAEs).[9] IrAEs can occur in all organs, with the endocrine glands, skin, and liver being relatively commonly involved, and rarely in the pulmonary, central nervous, and musculoskeletal systems.[10] A systematic analysis of 23 studies involving patients with NSCLC receiving ICIs, reported an overall incidence of irAEs of approximately 65%, with severe irAEs (grade 3 or higher) occurring in 14–21%.[11] Various factors such as autoantibodies, cytokines, T cells, and the microbiome are associated with irAEs, indicating diverse and heterogeneous mechanisms.[12] Most patients who develop irAEs recover with corticosteroids or immunosuppressive drugs; however, severe cases lead to treatment discontinuation and even death.[13] Therefore, predicting which patients are at risk of developing irAEs, particularly severe ones.

Single-cell RNA sequencing (scRNA-seq) has enabled the analysis of complex cellular heterogeneity within the tumors and their immune microenvironment, such as cancer cells, fibroblasts, and various immune cells.[14–16] In this study, we performed scRNA-seq on peripheral blood mononuclear cells (PBMC) collected from patients before ICI treatment to characterize immune cell heterogeneity and investigate mechanisms underlying ICI resistance and irAEs. Using scRNA-seq, we identified and characterized biomarkers that can predict ICI resistance and irAE severity before treatment. Our study facilitated the identification of appropriate patients likely to have a favorable response to ICIs or reduced irAE severity based only on PBMC collected before treatment. Ultimately, our research contributes to minimizing the risks associated with immunotherapy, enhancing treatment outcomes, optimizing patient care, and developing effective immunotherapeutic approaches.

METHODS

Patients and sample collection

This study included patients diagnosed with advanced NSCLC who underwent treatment with ICIs as monotherapy at Chungnam National University Hospital from March 2019 to October 2023. Patients with oncogenic driver mutations for which targeted therapies are recommended as first-line treatment (eg, *EGFR*, *ALK*) were excluded from the study. Patients received intravenous administration of atezolizumab (1,200 mg every 3 weeks), nivolumab (3 mg/kg body weight every 2 weeks), or pembrolizumab (2 mg/kg of body weight or 200 mg every 3 weeks). Treatment persisted until patients encountered severe adverse events (AEs), were confirmed to have investigator-assessed disease progression, or opted to withdraw informed consent. Patients anticipated to derive clinical benefit were allowed to continue treatment beyond radiologic disease progression. Peripheral blood samples were obtained from patients prior to ICI administration. PBMCs for scRNA-seq analysis were separated from whole blood using standard Ficoll-Paque (GE HealthCare, Uppsala, Sweden) density gradient centrifugation, frozen in freezing media, and stored in liquid nitrogen until use. All samples showed a high viability of about 90% on average after thawing. Plasma excluding cells was obtained by centrifugation at 4,000 rpm at 4°C for 10 min. The supernatant aliquot 1.5 mL e-tube and store at −80°C until use. Frozen plasma was thawed and centrifuged at 13,000 rpm at 4°C for 5 min before use in the experiment.

Response and adverse events evaluation

A response assessment with CT was performed every three cycles for patients treated with pembrolizumab or atezolizumab, and every four cycles for patients treated with nivolumab. The response to ICI treatment was assessed based on the Response Evaluation Criteria in Solid Tumors, V.1.1. The complete remission (CR) was defined as completion of ICI treatment for more than 2 years and CR of the disease. Primary resistance (priR) was defined as disease progression at the first response evaluation after ICI treatment. AR was defined as a continuous (complete or partial) objective response lasting at least 6 months after treatment but was discontinued within 2 years due to disease progression. irAEs were characterized as dysimmune toxicities resulting from immune system dysregulation, primarily affecting the skin, gastrointestinal tract, liver, endocrine glands, or lungs, though they could manifest in any tissue. AEs were assessed based on the National Cancer Institute Common Terminology Criteria for Adverse Events, V.4.0. Mild irAEs were categorized as grade 1, moderate as grade 2, and severe irAEs were defined as grade 3 or higher.

T-cell receptor sequencing preparation from patients with NSCLC PBMC

T-cell receptor (TCR) libraries were constructed using total RNA which is isolated from cryopreserved PBMCs of patients with NSCLC. As the protocol of the SMART-Seq Human TCR kit (Takara) was described, the first strand of TCR complementary DNA (cDNA) was generated and then two rounds of semi-nested PCR were performed to amplify TCR cDNAs. All the libraries were multiplexed and sequenced on the Illumina MiSeq to produce 301 bp paired-end reads.

Single-cell RNA-seq library construction

Library preparation for scRNA-seq was followed according to the Chromium Single Cell 3' Reagent Kits User Guide (V.3.1, 10x Genomics). Single-cell suspensions were filtered through a 40 µm Flowmi cell strainer (Bel-Art), counted using a Countess II automated cell counter (Thermo Fisher), and then loaded onto a microfluidic chip. In the Chromium Controller, cells were separated into Gel beads-in-EMulsion (GEMs) where polyadenylated RNAs in individual cells were tagged with a UMI (unique molecular identifier) and cell barcode. As soon as GEM generation was finished, reverse transcription was performed to produce barcoded cDNAs. cDNAs were amplified through PCR and amplified cDNAs were used for sequencing library construction. Briefly, cDNA amplicons were enzymatically fragmented, end-repaired, dA-tailed, and ligated with a sequencing adaptor. The final sequencing libraries were generated by sample index PCR and sequenced using a HiSeq 2500 (Illumina).

Single-cell RNA sequencing analysis

Raw base call files were demultiplexed using mkfastq application (Cell Ranger V.7.1.0) to make FASTQ files. Sequencing reads were mapped to the Ensembl genes (GRCh38) using the count application (Cell Ranger V.7.1.0) with default settings.[17] Quality control and basic downstream analyses were performed as in our previous studies.[18 19] To remove ambient RNA, the CellBender package (V.0.2.2) was used with default settings. Next, we used the following criteria at the cell-line analysis to filter out low-quality cells and genes: minimal expression of 200 genes per cell; maximum expression of 5,000 genes per cell; total expression less than 20,000 UMIs per cell; mitochondrial content less than 10%. Next, to remove double cells, the DoubletFinder package (V.2.0.3) was used per samples in compliance with 10x Genomics criteria indicating doublet probability per cell number.[20] Total 222,144 PBMC cells were obtained after filtering steps. Data were normalized using the "LogNormalize" method with a scale factor of 10,000 using the Seurat package (V.4.3.0).[21] ScaleData function of Seurat was used to regress out the number of UMI, the number of genes and per cent mitochondrial genes to remove unwanted sources of variation. Top 2,000 variably expressed genes were identified by FindVariableFeature function of Seurat with "vst" option. Batch effects between the samples were removed by using "RunHarmony" in the harmony package (V.0.1.1).[22] After the principal components analysis, cells were clustered using the FindClusters function of Seurat (resolution=0.4) on the basis of shared nearest neighbor using the identified 21 principal components. The cells were visualized by using Uniform Manifold Approximation and Projection (UMAP) embedding. After UMAP embedding, a total of 11 clusters were identified and annotated based on already unveiled markers information. Each cell type was subclustered and annotated based on well-known marker information. Differentially expressed genes (DEGs) between every pair of clusters were identified by using FindMarkers (p_val_adj<0.01 and avg_log2FC>1). Then, clusters were merged if the number of DEGs was less than 10 between two clusters. The marker genes were identified by using the FindAllMarkers function of Seurat with the Wilcoxon test (p_val_adj<0.01). DEGs used in the volcano plot, heatmap, and dotplot were identified (p_val_adj<0.05 and avr_log2>0.25). Pseudo-bulk analysis was performed using the AverageExpression function from the Seurat R package. Raw UMI count was used as input and pseudo time was calculated using the reduceDimension and orderCells function of Monocle2 (V.2.26.0). Through the differentialGeneTest function of Monocle2, trajectory patterns were determined. The significance of gene expression was calculated using the Wilcoxon rank-sum test in case compared between two groups, and the Kruskal-Wallis test was used in more than three groups.

TCR sequencing analysis

The TCR raw FASTQ data were subjected to processing using MIXCR (V.4.3.2).[23] The aligning of the raw data was processed through the align function within MIXCR. Subsequently, the assembly of CDR3 regions was performed using the assemble function in MIXCR. To identify the TCR diversity and clonality, the immunarch R package (V.0.9.0) was employed for visualization.[24] The TCR diversity and clonality were assessed using the repDiversity and trackClonotypes functions within the immunarch package, respectively.

Cell–cell communication analysis

CellPhoneDB (https://github.com/Teichlab/cellphonedb), a public repository of ligands, receptors and their interactions, was used to perform the cell–cell communication analysis.[25] Normalized UMI count and cluster identities were used as the input file for statistical_analysis function with a p value of 0.05. Visualization was done using ggplot2 R package. In addition to CEllPhoneDB, Nichenet was used to identify cell-to-cell interactions and targets that were

regulated by ligands.[26] Their interaction and target regulating potential were calculated using the Nichent database, and it was visualized by the pheatmap R package (V.1.0.12).

Gene co-expression network

Gene co-expression networks were constructed using the high-dimensional weighted gene co-expression network analysis (WGCNA) R package (V.0.28.1).[27] The parameter settings were configured in accordance with the manufacturer's instructions. The calculation of the weighted adjacency between genes was based on the Pearson correlation. To enhance the accuracy of the co-expression network, a soft power threshold of 4 was set. This threshold facilitated the removal of noise and weak connections, contributing to the construction of an accurate co-expression network. Each network was characterized by its biological pathways using DAVID. The differences in fold change were visualized using the ggplot2 R package.

BIOLOGICAL FUNCTIONS AND PATHWAYS

The inflammation and TNFA_NFKB1 score were calculated using the AddModuleScore function in Seurat. The genes comprising each module were from the MSigDB hallmark database.[28] A natural killer (NK) cell-mediated cytotoxicity pathway was obtained from KEGG (Kyoto Encyclopedia of Genes and Genomes).[29] The biological pathways in the heatmap were identified using Enrichr (https://maayanlab.cloud/Enrichr/) and DAVID (https://david.ncifcrf.gov/summary.jsp), which is a gene ontology web user interface.[30 31] Significant biological functions were selected applying to pathways, below a p value of <0.05. Heatmap was generated using "pheatmap" R package.

Plasma measurements of cytokines and cytotoxic effector molecules

The levels of plasma IL-1β, CXCL8 (IL-8) were determined using cytometric bead array (CBA) Enhanced Sensitivity Flex Set System (BD Biosciences, San Diego, California, USA) according to following the manufacturer's instructions. Plasma samples were thawed and pre-cleared by centrifuging at 13,000 rpm for 5 min. To measure the cytokines using 50 µL plasma, samples were analyzed on BD LSRFortessa X-20 (BD Biosciences, San Diego, California, USA). The data were analyzed using BD Biosciences CBA software. Plasma CXCL2 levels were measured using a Human CXCL2/GRO beta DuoSet ELISA (R&D Systems, catalog no. DY276-05). Plasma levels of interferon-gamma (IFN-γ) were quantified using an ELISA kit (Cat# DY285B-05, R&D Systems, Minneapolis, Minnesota, USA) in accordance with the manufacturer's protocol. Plasma levels of perforin and granzyme B were measured using selected targets from the LEGENDplex Human CD8/NK Panel (BioLegend, San Diego, California, USA), following the manufacturer's instructions. Data were acquired by flow cytometry and analyzed using the LEGENDplex Data Analysis Software.

RESULTS

Single-cell analysis of PBMCs in patients with NSCLC prior to ICI therapy

The baseline characteristics and efficacy outcomes of the patients undergoing ICI treatment are summarized in (online supplemental file 3). All participants had advanced stage III or IV NSCLC. The predominant histological types were adenocarcinomas (54.5%) and squamous cell carcinomas (33.3%). Regarding PD-L1 expression, 60.6% (20/33) of patients exhibited high expression, while 39.4% (13/33) showed low or no expression. Of the 33 patients included, none harbored driver mutations eligible for first-line targeted therapy such as EGFR or ALK. Most patients had received at least one prior systemic treatment. Excluding five patients who discontinued ICI due to AEs and were unevaluated for treatment response, seven of the remaining 28 patients achieved CR, 13 exhibited priR, and eight showed AR. Among the 33 patients, six experienced mild-to-moderate irAEs, while seven experienced severe irAEs. In total, 13 patients (39.4%) developed irAEs, with some experiencing more than one event. The most common irAEs were hepatitis (n=5), pneumonitis (n=4), and drug eruption (n=3). A detailed list of irAE types and corresponding Common Terminology Criteria for Adverse Events (CTCAE) grades is provided in (online supplemental table 1). To identify key candidates associated with the efficacy of ICIs and irAEs, we collected 33 baseline PBMC samples from patients with NSCLC before ICI therapy and scrutinized them at the single-cell level (figure 1A, B). Following a rigorous quality control process, 222,144 cells were obtained and divided into 11 distinct cell types (figure 1, online supplemental file 1). Each cell type was characterized using representative marker genes (online supplemental figure S1D).

Transcriptional profiling of immune cells reveals key pathways associated with complete response to ICIs

To investigate the immune cell profile linked to ICI efficacy, we analyzed cell proportion and biological pathway changes across three prognosis groups: CR, AR, and priR. CD4 T-cell proportions decreased, while CD8 T cells increased in AR compared with CR, although these changes were not statistically significant (figure 1D). Additionally, no significant differences in cell proportions were observed based on PD-L1 expression levels, tumor histology, previous treatment regimen (online supplemental figure S2A). In contrast, significant alterations in the biological functions were observed when comparing CR to priR (figure 2A). CD8 T cells in CR demonstrated a robust upregulation of biological pathways associated with immune reactions linked to a favorable prognosis

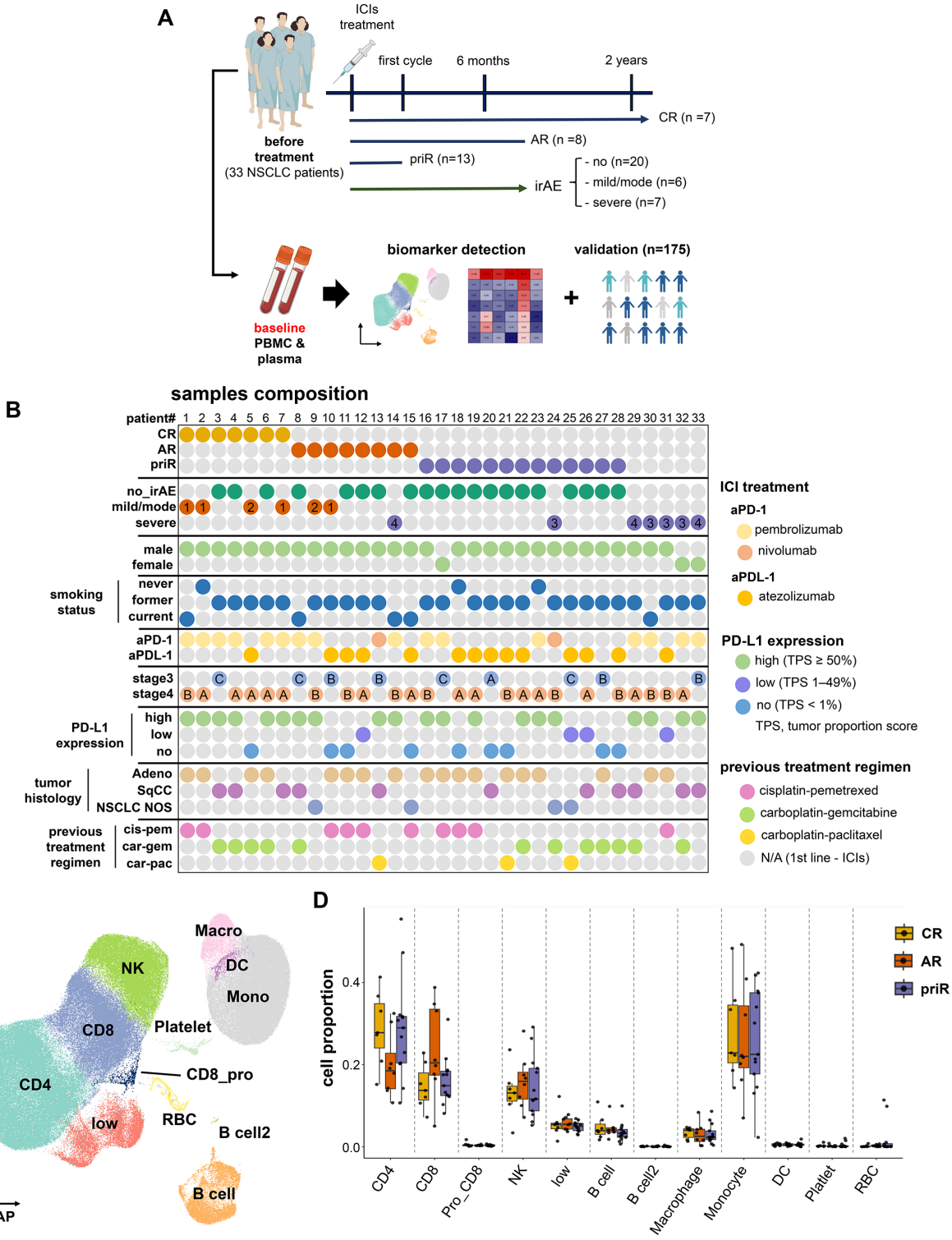

Figure 1 Comprehensive profiling of 33 patients with NSCLC PBMC prior to ICI therapy. (A) Workflow showing overall study design. (B) Clinical information of each patient included in our study. IrAE grades are indicated by a numerical value, and cancer stage are denoted by letter. (C) UMAP (Uniform Manifold Approximation and Projection) depicting 11 major cell types. Each cell type is labeled on the UMAP, and distinct colors represent individual cell types. (D) Box plot illustrating changes in the proportions of three ICIs prognosis groups (CR, AR, priR) in whole cell types. Each color indicates a specific prognosis group. Adeno, adenocarcinoma; AR, acquired resistance; aPD-1, anti-programmed cell death protein 1; aPD-L1, anti-programmed death-ligand 1; CD8_Pro, proliferating CD8 T cells; CR, complete remission; DC, dendritic cells; ICI, immune checkpoint inhibitor; irAE, immune-related adverse event; Macro, macrophages; Mono, Monocytes; NK, natural killer cells; NSCLC NOS, non-small cell lung cancer (NSCLC) not otherwise specified; PBMC, peripheral blood mononuclear cell; PD-1, programmed death-1; PD-L1, programmed death ligand 1; priR, primary resistance; SqCC, squamous cell carcinoma; TPS, tumor proportion score.

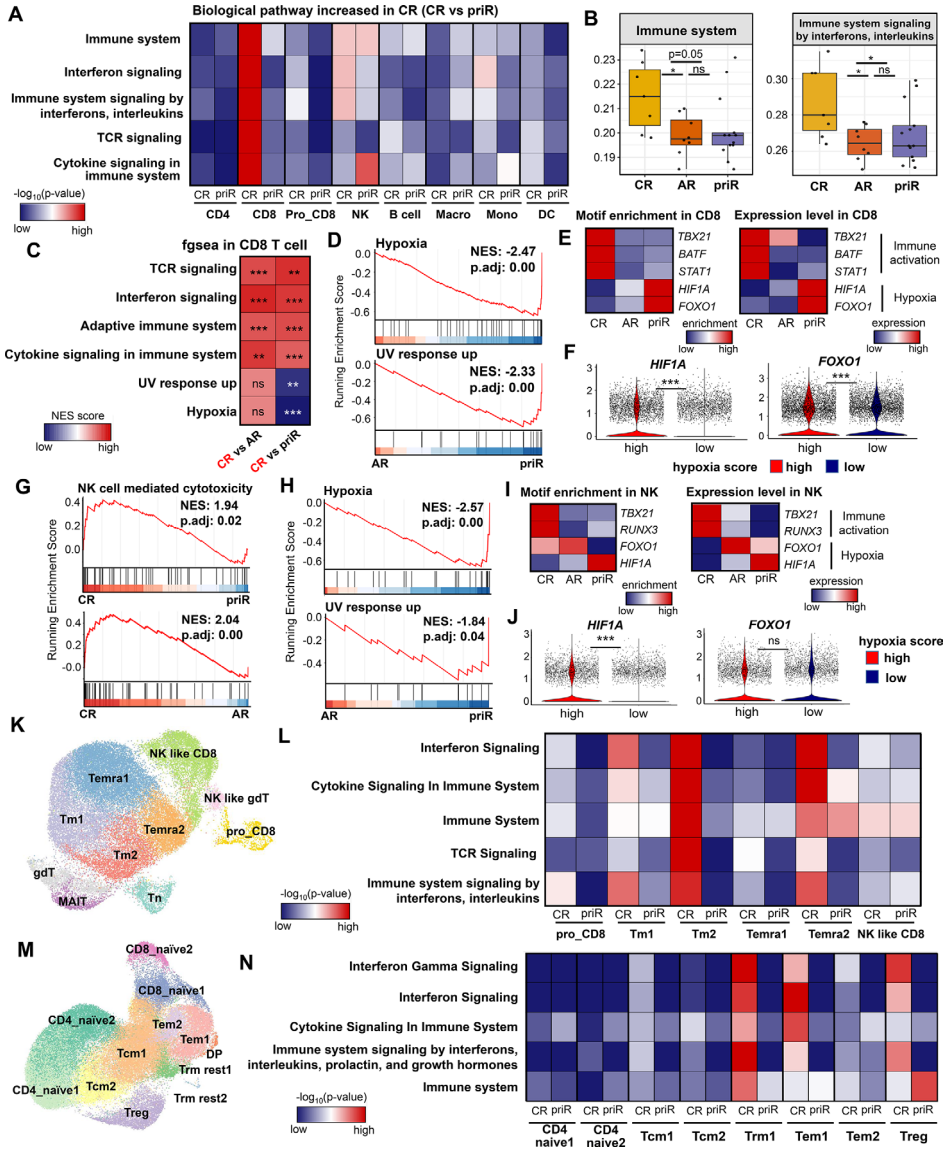

Figure 2 Profiling of 33 non-small cell lung cancer peripheral blood mononuclear cell samples and characterization associated with CR (A). Heatmap demonstrating the biological pathway of genes increased in CR compared with priR in all cell types. Color indicates values of significance (–$\log_{10}$(p value)). (B) Box plot illustrating each biological pathway score among the three ICI prognosis groups (CR, AR, priR) in CD8 T cells. Each color indicates a specific prognosis group. (C) Heatmap exhibiting the biological pathway of genes increased in CR compared with AR and priR in CD8 T cells. The asterisk indicates the significance, and the color shows normalization enrichment score. (D) The fgsea displaying gene set enrichment of hypoxia and UV response pathway variation between AR and priR in CD8 T cells. (E) Heatmap showing target motif enrichment (left) and gene expression (right) of the transcription factors in the CD8 T cells. The color indicates enrichment and expression levels. (F) Violin plot showing expression of *HIF1A* and *FOXO1* across the hypoxia scores. ∗p<0.05, ∗∗p<0.01, ∗∗∗p<0.001. (G) The fgsea displaying gene set enrichment of NK cell-mediated cytotoxicity pathway variation between CR and priR (upper) or CR and AR (lower) in NK cells. (H) The fgsea displaying gene set enrichment of hypoxia and UV response pathway variation between AR and priR in NK cells. (I) Heatmap showing target motif enrichment (left) and gene expression (right) of the transcription factors in the NK cells. The color indicates enrichment and expression levels. (J) Violin plot showing expression of *HIF1A* and *FOXO1* across the hypoxia scores. ∗p<0.05, ∗∗p<0.01, ∗∗∗p<0.001. (K) UMAP depicting 10 subtypes of CD8 T cells. Each cell type is labeled on the UMAP, and distinct colors represent individual cell types. (L) The heatmap illustrating the biological pathway of genes increased in CR compared with priR in CD8 T-cell subtypes. Color indicates values of significance (–$\log_{10}$(p value)). (M) UMAP depicting 12 subtypes of CD4 T cells. Each cell type is labeled on the UMAP, and distinct colors represent individual cell types. (N) The heatmap illustrating the biological pathway of genes increased in CR compared with priR in CD4 T-cell subtypes. Color indicates values of significance (–$\log_{10}$(p value)). AR, acquired resistance; CR, complete remission; DC, dendritic cells; DP, double positive; fgsea, fast gene set enrichment analysis; Macro, macrophages; Mono, Monocytes; NES, normalized enrichment score; NK, natural killer cells; priR, primary resistance; pro_CD8, proliferating CD8 T; Tcm, central memory CD4 T; TCR, T-cell receptor; Tem, effector memory CD4; Temra, terminally differentiated effector CD8; Tm, memory CD8 T; Tn, naive CD4 T; Treg, regulatory CD4; Trm rest, tissue resident memory resting CD4; UMAP, Uniform Manifold Approximation and Projection; UV, ultraviolet radiation.

for ICI therapy, whereas no significant differences were observed between AR and priR (figure 2A and B; online supplemental figure S3A).[32 33] While pathways related to hypoxia and ultraviolet radiation (UV) responses, which suppress immune suppression,[34 35] were more pronounced in priR than in CR, with no significant differences between AR and CR (figure 2C). Direct comparison of AR and priR confirmed elevated hypoxia and UV responses in priR (figure 2D). Additionally, priR showed upregulated expression of *HIF1A* and *FOXO1*, which are transcription factors (TFs) activated in hypoxic environments, along with enrichment of their target motifs (figure 2E).[36–38] Conversely, the gene expression and target motif enrichment of immunity-activating TFs, such as *TBX21*, *BATF*, and *STAT1*, were increased in the CR group (figure 2E). Furthermore, we observed a positive correlation between *HIF1A* and *FOXO1* expression and increased hypoxia scores in priR patients and identified the elevation of protumorigenic inflammatory activity according to the upregulation of hypoxia in priR cells (online supplemental figure S3B).[39]

In NK cells, increased NK cell-mediated cytotoxicity was observed in CR compared with that in both AR and priR (figure 2G). Additionally, consistent with the CD8 T-cell results, hypoxia and UV response pathways were upregulated in priR compared with AR (figure 2H and online supplemental figure S3B). While the expression and target motifs of TFs, such as *TBX21* and *RUNX3*, which promote NK cell activation, were enriched in the CR group, *HIF1A* expression increased in the priR group (figure 2I). Furthermore, *HIF1A* was upregulated with increasing hypoxia scores in priR, but not in *FOXO1* (figure 2J).

Given the robust increase in immune reactions observed in CR of CD8 T cells, we further subclustered CD8 T cells to scrutinize (figure 2K and online supplemental figure S3C). While the proportion of each subtype among the three prognosis groups showed no significance, biological pathway changes were markedly altered between CR and priR, particularly in memory CD8 T cell2 (Tm2) (figure 2L and online supplemental figure S3D). Tm2 cells in the CR exhibited predominant activation of immune-related signals, including immune system and cytokine signaling, compared with the other two groups (figure 2L and online supplemental figure S3E). These increases were also observed in memory CD8 T cell1 and terminally differentiated effector memory CD8 T cells2, where immune-related pathways were upregulated in CR compared with AR and priR within these cell types (figure 2L and online supplemental figure S3F and 3G).

Despite no significant differences in biological pathways being observed between CR and priR in whole CD4 T cells, CD4 T-cell subtype-level analysis revealed distinct biological pathway differences between CR and priR (figure 2A, M and N; online supplemental figure S4A). While tissue-resident memory resting CD4 (Trm rest1) cells showed no proportional changes among the three prognostic groups, genes that increased in CR were strongly associated with immune reactions, including interferon and cytokine signals (figure 2N and online supplemental figure S4B, C). Additionally, immune activation pathways were intensified in CR of effector memory CD4 and regulatory CD4 cells, with both subtypes displaying upregulation of these pathways in CR compared with AR and priR (figure 2N and online supplemental figure S4D, E).

Collectively, immune activation responses, such as interferon and cytokine signaling, were significantly increased in CR compared with both AR and priR, whereas hypoxia-related signaling was notably prominent only in priR.

Discovery of key factors linked to ICI therapy prognosis in T and NK cells

Based on the CR-specific characterization confirmed in previous results, we conducted an analysis to identify key factors associated with ICI prognosis. We first examined Tm2 cells, which exhibited the most pronounced immune characteristic differences in CR of CD8 T cells (figure 2L). To explore genes specific to CR and associated with immune reactions, we performed a WGCNA to examine the co-expression patterns between transcripts in Tm2. We identified five modules, with the green module being significantly elevated in the CR group (figure 3A). Genes in the green module were associated with T-cell activation and immune responses (figure 3A). Moreover, this module showed a distinct increase in CR compared with both priR and AR among the four modules (figure 3B and online supplemental figure S5A). We further narrowed down the candidates by selecting CR-specific upregulated genes within the green modules and identified 52 genes (figure 3C, D). The expression of these genes was validated using public baseline PBMC data, where we isolated CD8 T cells and observed an elevation of these 52 gene set scores in the Tm of the ICI response group of public data (figure 3E and online supplemental file 1).[40] Among the 52 genes, we identified three main candidates: *NKG7*, *GZMH*, and *PRF1*. These genes were selected based on their significant increases in both the CR of our data and the response group of the public dataset (figure 3F and G). Interestingly, we found that these genes are involved in antitumor activities by inducing inflammation and apoptosis in tumor cells and aiding granzyme delivery.[41–43] Their expression was detected in almost all CD8 T cells regardless of subtype, and both datasets confirmed their increased expression in the ICI response group (CR and response) (online supplemental figure S5E-G). Additionally, we investigated their expression changes under different conditions, such as PD-L1 expression, tumor histology, and treatment regimen. Given the unbalanced sample distribution in each condition (online supplemental file 1), we analyzed specific groups and found that their expression was elevated in the CR, regardless of condition differences (online supplemental figure S5K-M). Next, to validate the marker's expression in a large cohort, we performed a CBA assay on plasma samples from 122 patients and identified expression changes of perforin, which showed

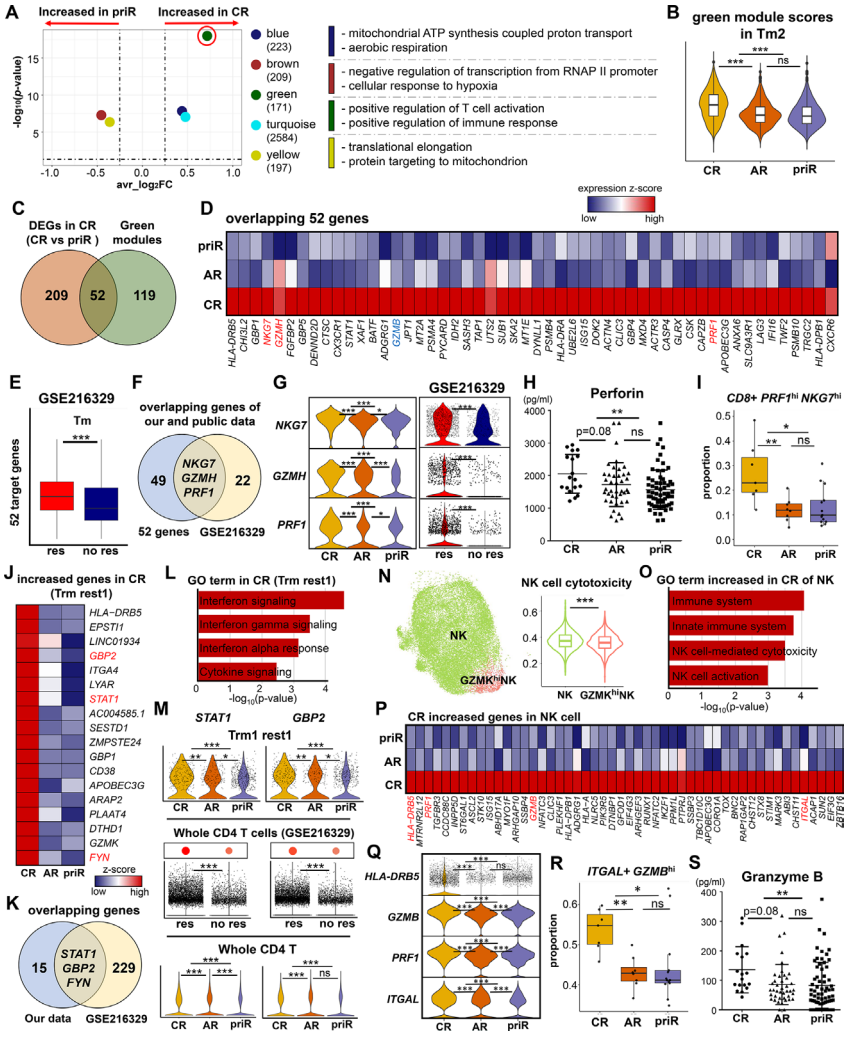

Figure 3 Discovery of key candidates linked to ICI therapy prognosis in CD8 T and CD4, and NK cells (A). Volcano plot displaying differentially expressed modules, which resulted from weighted gene correlation network analysis, between CR and priR. Each color indicates each module, and numbers represent the number of genes belonging to each module. The x-axis represents avg_log2FC and y-axis shows –log(p_value). (B) Violin plot indicating gene set scores of genes belonging to a green module in memory CD8 T cell2. Each color represents each prognosis group. (C) Venn diagram showing the number of overlapping genes between CR specifically increased genes and green module genes. (D) Pseudo-bulk analysis showing expression levels of 52 genes overlapping between CR in CD8 T cells and green modules. The color indicates expression levels of each gene among different prognosis groups. (E) Box plot illustrating 52 gene scores between the ICI response group and no response groups from public data (GSE216329). (F) Venn diagram showing the number of overlapping genes between our data and public data. (G) Violin plot indicating *NKG7*, *GZMH*, and *PRF1* expression levels in memory CD8 T cells of our data (left) and public data (right). (H) Bee swarm plot indicating perforin expression levels among three prognosis groups. The y-axis indicates expression levels. ∗p<0.05, ∗∗p<0.01, ∗∗∗p<0.001. (I) Box plot illustrating changes in the proportion of cells with higher expression levels than an average expression of *PRF1* and *NKG7* among CD8A positive cells. (J) Pseudo-bulk analysis showing expression levels of 18 genes increased in CR from Trm rest1 of CD4 T cells. The color indicates expression levels of each gene among different prognosis groups. (K) Venn diagram showing the number of overlapping genes between our data (18 genes) and public data. (L) Bar plot presenting biological pathways in CR of a Trm rest1 of CD4 T cells. The x-axis indicates –log10(p value). (M) Violin plot indicating *STAT1* and *GBP2* expression levels between three prognosis groups in Trm rest1 (upper), whole CD4 T cells from public data (middle), and whole CD4 T cells from our data (lower). (N) UMAP depicting subtypes of NK cells (left) and violin plot showing NK cell-mediated cytotoxicity score (Kyoto Encyclopedia of Genes and Genomes) in NK subtypes. (O) Bar plot presenting biological pathways in CR of an NK subtype. The x-axis indicates –log10(p value). (P) Pseudo-bulk analysis showing expression levels of differentially increased in CR of NK cells. The color indicates expression levels of each. (Q) Violin plot indicating *HLA-DRB5*, *GZMB*, *PRF1*, and *ITGAL* expression levels between three prognosis groups in NK cells. (R) Box plot illustrating change in the proportion of NK cells with expression levels above an average expression of *GZMB* and positive expression of *ITGAL*. ∗p<0.05, ∗∗p<0.01, ∗∗∗p<0.001. (S) Bee swarm plot indicating granzyme B expression levels among three prognosis groups. The y-axis indicates expression levels. ∗p<0.05, ∗∗p<0.01, ∗∗∗p<0.001. AR, acquired resistance; CR, complete remission; DEG, differentially-expressed gene; GO, gene ontology; ICI, immune checkpoint inhibitor; NK, natural killer; priR, primary resistance; Trm rest1, tissue-resident memory resting CD4; UMAP, Uniform Manifold Approximation and Projection.

the most distinct expression differences between prognosis groups in single cell data (figure 3G and online supplemental figure 5SN). Its expression was significantly increased in the CR compared with priR, with a similar trend observed in the AR (figure 3H). Then, to further enhance discriminative accuracy, we combined biomarkers. Among CD8-positive cells, those with high expression of both *PRF1* and *NKG7* or *PRF1* and *GZMH* were predominantly observed in CR cells compared with AR and priR cells (figure 3I). Moreover, combining all three candidates resulted in significant discrimination accuracy among CR, AR, and priR (online supplemental figure S5O).

In CD4 T cells, we also identified candidates that were commonly upregulated in response to ICI in both our data and public data.[40] Specifically, we identified 32 genes that were upregulated in CR from Trm rest1 that previously exhibited an active immune response in CR (figures 2N and 3J). Among these, *STAT1*, *GBP2*, and *FYN* were commonly upregulated in the response groups of both our data and the public datasets (figure 3K). Previous studies have shown that these genes are closely associated with multiple immune responses. Given the marked increase in IFN signaling during CR, we focused on *STAT1* and *GBP2*, which are strongly linked to the interferon pathway (figure 3L). We observed a significant increase in these genes within CR of Trm rest1 (figure 3M). Since the CD4 Trm rest1 cell type was not present in the public data, we analyzed total CD4 T cells in both datasets and confirmed their upregulation in CR (figure 3M, online supplemental figure S6A, B). Notably, these genes were elevated in almost all CR groups, regardless of PD-L1 expression, tumor histology, or treatment regimen (online supplemental figure S6C-E). Furthermore, the combination of these biomarkers enhanced the discrimination accuracy for CR, AR, and priR (online supplemental figure S6F).

In addition to CD4 T cells, we explored NK cells, which are known for their cytotoxicity against cancer cells. Considering the high population and cytotoxicity scores, we closely examined the NK cell subtypes (figure 3N, online supplemental figure S6G, H). Given the cell population and the high score of NK cell-mediated cytotoxicity, we scrutinized NK cells but not $GZMK^{hi}$ NK cells (figure 3N and online supplemental figure S6H). Genes upregulated in the CR of NK cells indicated the activation of immune responses and NK cell-mediated cytotoxicity (figure 3O). Among the various genes that were distinctly upregulated in the CR of NK cells, four key candidates were identified: *HLA-DRB5*, *GZMB*, *ITGAL*, and *PRF1* (figure 3P). *HLA-DRB5* was reported to be expressed on activated NK cells, and *ITGAL*, *GZMB*, and *PRF1* were revealed to be involved in regulating NK cell infiltration and antitumor activity.[44–47] These genes were significantly elevated in the CR of NK cells, and the combination of biomarkers (*ITGAL* and *GZMB*) allowed clear discrimination between priR and CR (figure 3Q and R). Similar to CD4 and CD8 T cells, these marker genes were increased in almost all CR samples, irrespective of specific conditions, such as PD-L1 expression level or tumor histology and treatment regimen (online supplemental figure S6I-K). Interestingly, among the four candidates, *GZMB* expression was increased in CR, not only in NK cells but also in Tm2 of CD8 T cells and whole CD8 T cells (figure 3D and Q; online supplemental figure S6L). Given that *GZMB* was a secreted cytokine, we identified its expression changes using a CBA assay. The granzyme B expression was distinctly elevated in the CR compared with the AR and priR, and patients with higher granzyme B expression were majorly composed of CR (online supplemental file 1 and online supplemental figure 6SM).

Identification of irAE biomarkers in monocytes strongly associated with severe irAE

To identify biomarkers for predicting irAEs, we conducted a comprehensive analysis according to irAEs severity. We classified the patients into three categories: no irAEs, mild-to-moderate irAEs, and severe irAEs. We observed no significant differences in the proportions of the three irAE groups among various cell types (online supplemental figure S7A). However, monocytes exhibited the most distinct increase in severe irAEs compared with the other two groups and constituted the predominant cell type in the severe irAE group (online supplemental figure S7A). Additionally, monocytes displayed the highest inflammation score among all cell types, with inflammation pathways being particularly pronounced in the severe irAE group compared with the other two groups, but showed no significant difference between the no irAE and mild/moderate irAE groups (figure 4A, online supplemental figure S7B, C). Increased active inflammation in severe irAE is associated with hypoxia,[48] and in our study, we observed an increase in hypoxia-related pathways in severe irAE compared with no irAE and mild/moderate irAE (figure 4B and online supplemental figure S7D). Next, we identified the genes that were specifically upregulated in severe irAEs and were relevant to inflammatory responses (figure 4C). From the various genes, we selected five candidates, *CXCL8*, *CXCL2*, *IL1B*, *CCL3*, and *EREG*, which are involved in diverse immune responses and are upregulated in severe irAEs (figure 4C and D). These genes were specifically expressed in monocytes and indicated a strong correlation with the inflammatory response, which was elevated in monocytes, particularly in severe irAEs (figure 4E and online supplemental figure S7E). Furthermore, these candidates showed increased expression in the group with heightened inflammation (figure 4F). Notably, their expression was upregulated in severe irAE across all conditions. Although we investigated expression changes in specific conditions due to sample distribution, their expression was significantly elevated in all severe irAE patients of diverse conditions except for NSCLC not otherwise specified (NOS), with strong upregulation of *CXCL8* and *IL1B* (online supplemental figure S7F-I).

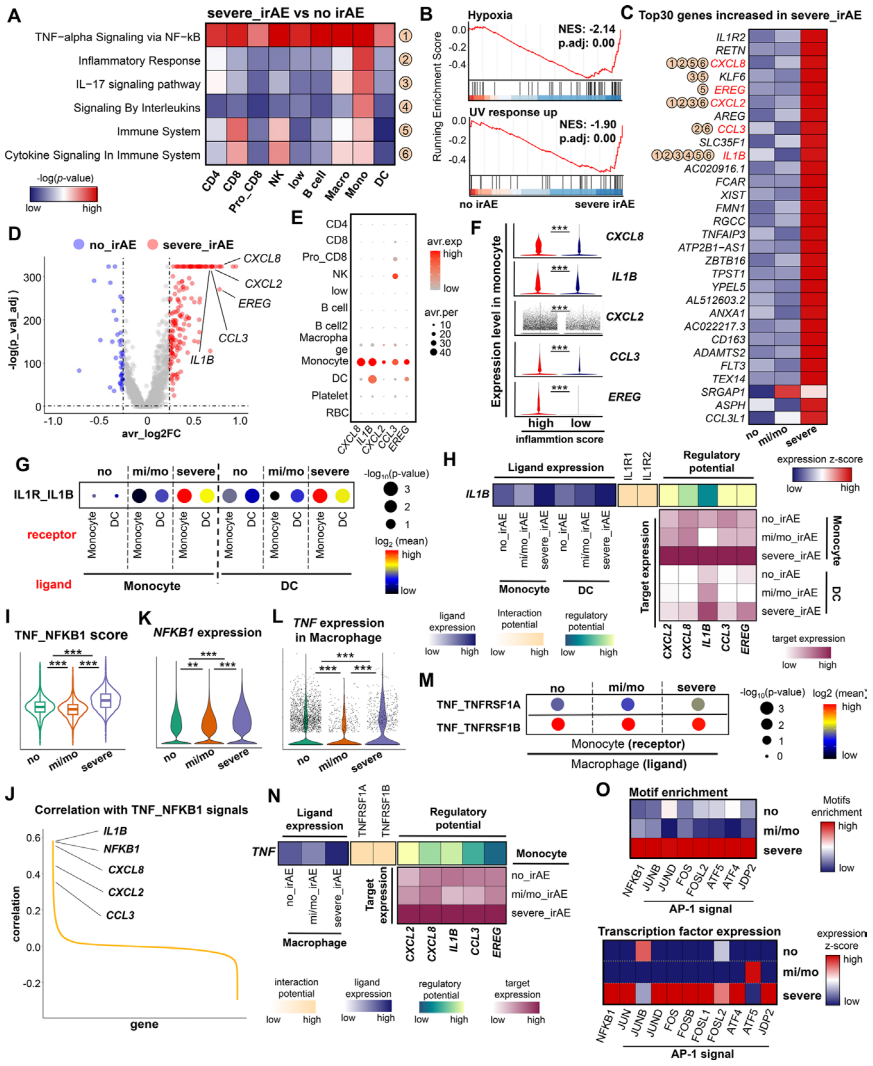

Figure 4 Identification of irAE biomarkers in monocytes strongly associated with irAE severity (A). The heatmap illustrating the biological pathway of genes increased in severe_irAE compared with no_irAE in all cell types. The color visualizes values of significance (–$\log_{10}$(p value)). (B) The fgsea displaying gene set enrichment of hypoxia and UV response pathway variation between no irAE and severe irAE in monocytes. (C) Pseudo-bulk analysis showing gene expression levels specifically increased in severe_irAE of monocytes. The color indicates expression levels of each gene among different irAE groups. Biological pathways associated with each gene are denoted by a number. The main candidate genes were highlighted in red color. (D) Volcano plot displaying gene expression changes between severe_irAE and no_irAE. The main candidate genes are labeled on the plot. The red and blue dots indicated increased genes in severe_irAE and no_irAE, respectively. The x-axis represents avg_$\log_2$FC and y-axis shows –$\log_{10}$(p_val_adj). (E) Bubble plot showing expression levels of five main candidates (*CXCL8*, *IL1B*, *CXCL2*, *CCL3*, *EREG*) in whole cell types. The color and dot size represent expression levels and per cent of cells expressing each gene, respectively. (F) Violin plot showing expression of main candidate genes according to the inflammation score levels. ∗p<0.05, ∗∗p<0.01, ∗∗∗p<0.001. (G) Dot plot indicating IL1R-IL1B interaction intensities between three irAE groups of monocytes and DCs. The dot color represents interaction intensities (log2(mean)), and dot size indicates interaction significance. (H) Heatmap displaying interaction potential and ligand and target gene expression. Ligand expression indicates *IL1B* expression levels in monocytes and DC between the three irAE groups. Regulatory potential represents the likelihood that ligands regulate the target genes. Target expression indicates the expression levels of target genes. (I) Expression level of TNFA_NFKB1 score between three irAE groups in monocytes. Each color represents each irAE group. (J) Line plot demonstrating the correlation between TNF_NKFB1 score and whole genes in monocytes. The main candidate genes are labeled on the plot. (K) Violin plot indicating *NFKB1* expression levels in monocytes. (L) Violin plot indicating *TNF* expression levels in macrophages. (M) Dot plot indicating TNF-TNF receptor interaction intensities between three irAE groups of monocytes and macrophages. The dot color represents interaction intensities (log2(mean)), and dot size indicates interaction significance (–$\log_{10}$(p value)). (N) Heatmap displaying interaction potential and ligand and target gene expression. Ligand expression indicates *TNF* expression levels between the three irAE groups in macrophages. Regulatory potential represents the likelihood that ligands regulate the target genes. Target expression indicates the expression levels of target genes. (O) Heatmap showing target motif enrichment (upper) and gene expression (lower) of the transcription factors in the monocytes. The color indicates enrichment and expression levels. DC, dendritic cell; fgsea, fast gene set enrichment analysis; irAE, immune-related adverse event; NES, normalized enrichment score; UV, ultraviolet radiation.

Next, we examined cell–cell interactions to elucidate the underlying mechanisms contributing to the elevation of candidates associated with severe irAEs. We focused on *IL1B*, which is involved in the pro-inflammatory response and increased in severe irAEs (figure 4C and D). Its receptors, *IL1R1* and *IL1R2*, were specifically expressed in monocytes and dendritic cell (DC), and they were distinctly upregulated in severe irAEs (online supplemental S8A and 8B). Intriguingly, we noted progressive intensification in the interaction between these cells, from no irAEs to severe irAEs (figure 4G). Through ligand-target analysis, we found that *IL1B* showed strong regulatory potential modulating the candidate genes, revealing a close association between the IL1B-IL1R interaction and the candidate genes (figure 4H).

Next, we examined the TNF_NKFB1 signaling pathway, which showed the greatest increase in severe irAE compared with no irAE in almost all cell types (figure 4A). This pathway was activated within monocytes and intensified in severe irAEs among the three irAE groups (figure 4I and online supplemental file 1). Furthermore, we observed a strong correlation between TNF_NKFB1 signaling and candidate genes such as *IL1B* and *CXCL8* within monocytes (figure 4J). Notably, *NFKB1*, the pivotal TF orchestrating this signaling cascade, displayed a marked increase in severe irAE and exhibited a significant correlation with the TNF_NKFB1 signaling (figure 4J and K). Additionally, we found that the ligand inducing this signal, *TNF*, was distinctly expressed in macrophages, and its expression increased in severe irAEs (figure 4L and online supplemental figure S8D). Similar to monocytes, *TNF* expression was elevated in almost all severe irAEs regardless of specific conditions, such as PD-L1 expression level, tumor histology and treatment regimen (online supplemental S8E-G). We also detected an increased interaction between TNF and its receptor TNFRSF1A, with the downstream targets induced by this interaction actively increasing in severe irAEs (figure 4M and N). Furthermore, the TNF interaction exhibited high regulatory potential in modulating the expression of targets identified in this study (figure 4N). Additionally, we confirmed that both transcript expression and motifs of NFKB1 and AP-1, the major TFs regulating inflammation-related signals activated by the TNF and IL1B interaction, were increased in severe irAE (figure 4O).

Validation of plasma cytotoxic effector molecules associated with irAE severity in a large cohort

Considering severity, expression specificity, and the involvement of biological functions, we provided candidates for predicting irAEs. While *CXCL8* and *IL1B* alone could predict irAE severity, cases in which both genes were positive demonstrated enhanced prediction accuracy (figure 5A). Additionally, the inclusion of one additional marker (*CCL3* or *EREG*) alongside *CXCL8* and *IL1B* further improved prediction accuracy (figure 5B). Notably, the expression of each gene or gene combination remained unaffected by PD-L1 expression or treatment regimen, while IL1B tended to increase in patients with squamous cell carcinoma (online supplemental figure S9A–C).

To validate our findings in a large cohort, we conducted a CBA using baseline plasma samples from 175 patients with NSCLC (figure 5C). We observed significant increases in CXCL8 and IL1B expression in patients with severe irAEs compared with those with no irAEs and mild/moderate irAEs (figure 5D and E). In addition, we observed an increase in CXCL2 expression in severe irAE compared with no irAE, although there was no statistically significant difference between severe irAE and mild/moderate irAE (figure 5F). Moreover, when all three groups were compared simultaneously, we identified distinctly elevated expression levels of CXCL8 and IL1B in patients with severe irAEs (figure 5G). Although CXCL2 expression did not reach statistical significance, an increasing trend was noted across groups (figure 5G). Consistent with the scRNA-seq results, in the larger cohort, we identified that patients who exhibited high expression levels of CXCL8 and IL1B predominantly had severe irAEs (figure 5H). Additionally, simultaneously high expression of both CXCL8 and IL1B was mainly confirmed in patients with severe irAEs, and we obtained similar results when defining high expression above the median value considering sample heterogeneity (figure 5I). Additionally, the proportion of patients with high expression of other gene combinations, such as CXCL8/CXCL2 and IL1B/CXCL2, was also significantly higher in severe irAEs compared with no or mild/moderate irAEs (online supplemental figure S9D, SE). Collectively, we identified effective candidate biomarkers, particularly CXCL8 and IL1B, for predicting irAE severity.

Identification of irAE severity biomarkers in CD8 T cells

Expanding our analysis beyond myeloid cells, we investigated the factors associated with the irAEs severity in lymphocytes. Referring to previous studies suggesting an elevation in IFNG levels with irAE severity, we examined *IFNG* expression in lymphocytes.[49] *IFNG* was specifically expressed in CD8 T, pro_CD8 T, and NK cells and was increased in severe irAE compared with the other two groups (figure 6A and online supplemental figure S10A). Moreover, its expression was pronounced in the severe irAE within CD8 T and NK cells across almost all conditions, such as PD-L1 expression, tumor histology, and treatment regimen (online supplemental figure S10B-D). Interestingly, *IFNGR1* and *IFNGR2*, the receptors of IFNG, were distinctly expressed in monocytes, macrophages, and DC cells, with increased expression in severe irAE (figure 6B and online supplemental figure S10E). The intensity of IFNG-IFNGR interactions progressively increased in severe irAEs in all cell types, with the most pronounced increase in the monocytes from severe irAE (figure 6C). We noted that IFNG-IFNGR demonstrated a high regulatory potential for the target genes we found in this study, implying that the

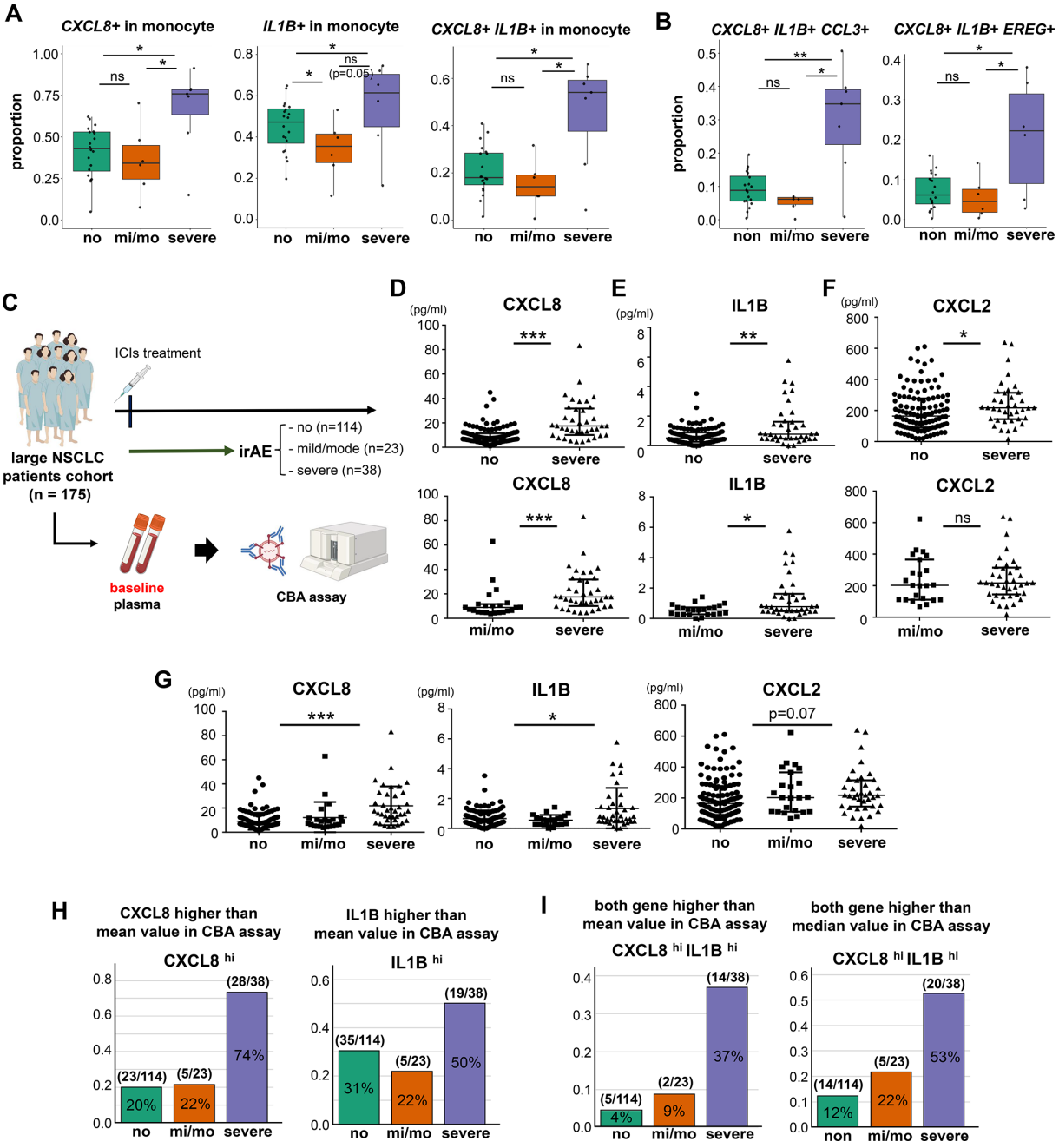

Figure 5 Validation of irAE severity biomarkers in large cohorts (A). Box plot illustrating changes in the proportion of cells expressing each gene *CXCL8* (left) and *IL1B* (middle) or both genes (right) among three irAE groups of monocytes. (B) Box plot illustrating changes in the proportion of cells expressing all three genes (*CXCL8*, *IL1B*, and *CCL3* or *CXCL8*, *IL1B*, and *EREG*) in three irAE groups of monocytes. (C) Workflow of CBA for the validation in a large cohort composing 175 patients with NSCLC prior to treatment. (D–F) Bee swarm plot indicating CXCL8 (D), IL1B (E), and CXCL2 (F) expression levels between no_irAE and severe_irAE (upper) or mild-to-moderate_irAE and severe_irAE (lower). The y-axis indicates expression levels. *p<0.05, **p<0.01, ***p<0.001. (G) Bee swarm plot indicating CXCL8 (left), IL1B (middle), and CXCL2 (right) expression levels among three irAE groups. The y-axis indicates expression levels. *p<0.05, **p<0.01, ***p<0.001. (H) Bar plot indicating proportion changes of cells showing higher expression levels than mean expression of CXCL8 (left) or IL1B (right) in CBA assay. (I) Bar plot indicating proportion changes of cells showing higher expression levels than average expression (left) or median expression (right) of CXCL8 and IL1B in CBA assay. CBA, cytometric bead array; ICI, immune checkpoint inhibitor; irAE, immune-related adverse event; NSCLC, non-small cell lung cancer.

activated IFNG-IFNGR interaction induced various target genes associated with inflammation, particularly in severe irAE monocytes (figure 6D). However, the CBA results showed no significant differences in IFN-γ expression between the irAE groups (online supplemental figure S10F). Although IFN-γ expression did not show expression differences in plasma,

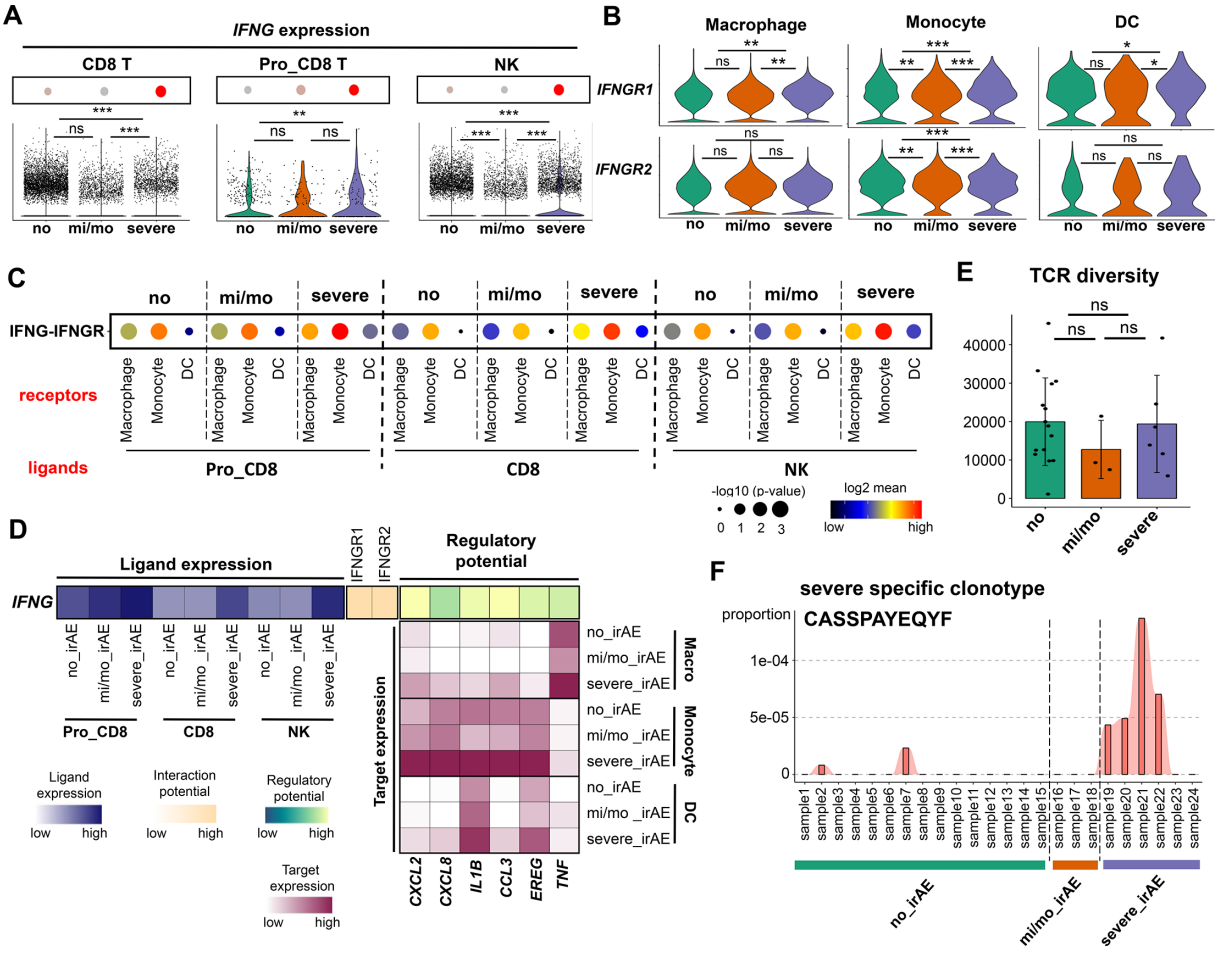

Figure 6 Identification of irAE severity biomarkers in CD8 T cells (A). Bubble plot and violin plot illustrating expression levels of *IFNG* in CD8 (left), Pro_CD8 (middle), and NK cells (right). (B) Violin plot indicating *IFNGR1* and *IFNGR2* expression levels between the three irAE groups of macrophages and monocytes, and DC. (C) Dot plot indicating IFNG-IFNGR interaction intensities between three irAE groups in various cell types. The dot color represents interaction intensities (log2(mean)), and dot size indicates interaction significance. (D) Heatmap displaying interaction potential, ligand, and target gene expression. Ligand expression indicates *IFNG* expression levels between the three irAE groups. Regulatory potential represents the likelihood that ligands regulate the target genes. Target expression indicates the expression levels of target genes. (E) Box plot illustrating TCR diversity among three irAE groups. The dot represents each sample. (F) Bar plot showing a TCR clonotype specifically identified in severe irAE. The x-axis indicates each sample, and the y-axis indicates the proportion of each clonotype in each sample. DC, dendritic cell; irAE, immune-related adverse event; NK, natural killer; TCR, T-cell receptor.

considering the high expression of receptors and interaction intensity in severe irAE, IFNG-IFNGR interaction may influence other immune cells, such as myeloid cells, contributing to severe irAEs (figure 6C and D).

Lastly, beyond biomarker discovery through transcriptional changes, we identified irAE severity-specific clonotypes using TCR sequencing at the bulk level in baseline PBMCs from 25 patients. Although TCR diversity was not significantly different among the three groups, we identified a few clonotypes unique to patients with severe irAEs (figure 6E and F, online supplemental figure S10G). These clonotypes were exclusive to patients with severe irAEs, suggesting the potential for TCR stimulation from various immune reactions in severe irAEs.

Unveiling biomarkers for favorable prognosis and reduced irAEs

Given that many patients in the CR group, associated with a favorable prognosis, had mild/moderate irAEs, these findings suggest that a mild immune response can effectively activate immunity and enhance antitumor effects (figure 7A and online supplemental figure S11A). In CD8 T cells from patients with mild/moderate irAEs, we observed the activation of immune system pathways associated with a favorable prognosis in the CR group, including NK-mediated cytotoxicity and T-cell activation pathways (figure 7B). Since mild/moderate irAEs consist of two prognostic groups (CR and AR), we investigated genes identified as CR-specific in both mild/moderate irAE and all irAE samples consisting of all prognostic groups (figure 7C). We identified 48 overlapping genes that were specific to CR (figure 7C). These genes were

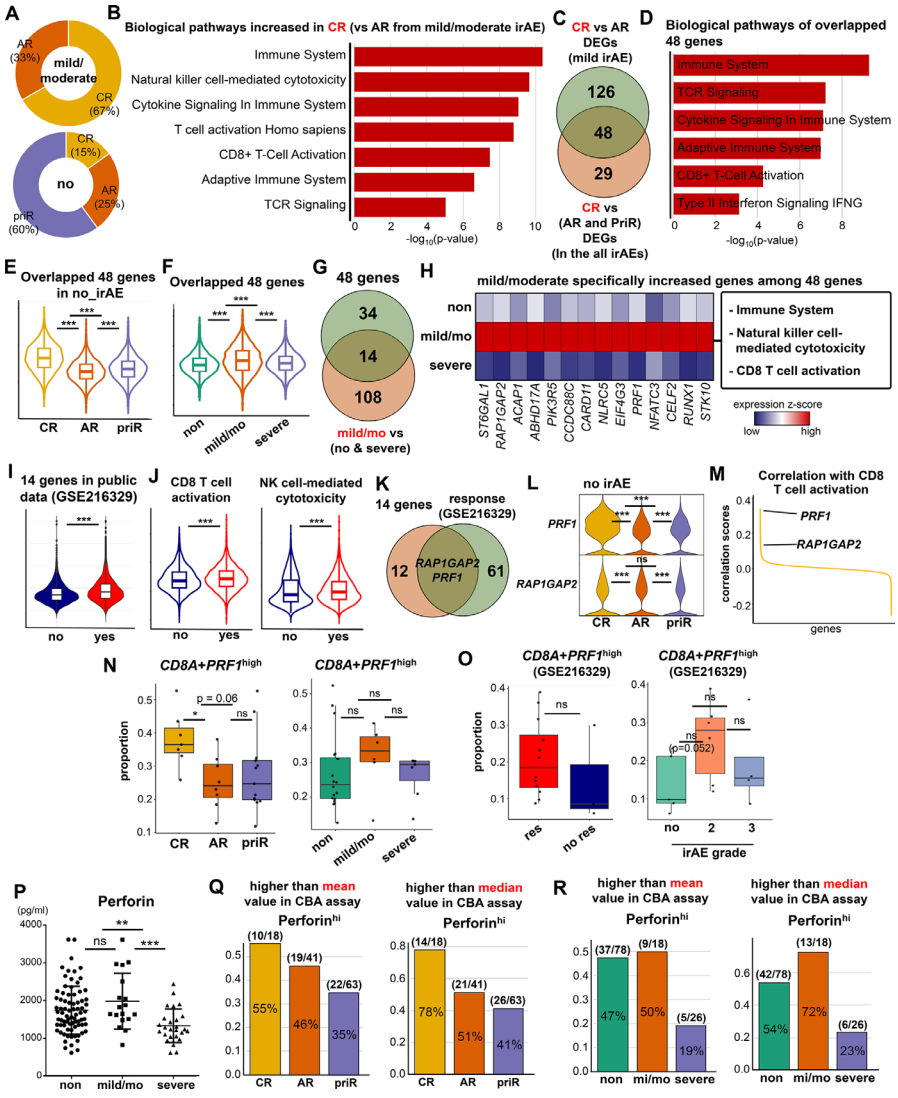

Figure 7 Discovery of biomarkers indicating good prognosis and less irAE (A). Donut plot showing the composition of samples indicating prognosis in the mild/moderate irAE and no irAE groups, respectively. (B) Bar plot showing biological pathways activated in CR compared with AR in the mild/moderate irAE group of CD8 T cells. The x-axis indicates –log10(p value). (C) Venn diagram showing the number of overlapping genes upregulated in the CR of mild/moderate irAE group within CD8 T cells, and genes upregulated in CR (vs AR and priR of all irAE group within CD8 T cells. (D) Bar plot showing biological pathways of overlapped 48 genes from (C). The x-axis indicates $-\log_{10}$(p value). (E) Violin plot indicating overlapped 48 genes score between the three prognosis groups within CD8 T cells from no_irAE samples. (F) Violin plot indicating overlapped 48 genes score between the three irAE groups within CD8 T cells. (G) Venn diagram showing the number of overlapping genes between 48 genes and genes upregulated in mild/moderate irAE (compared with severe irAE and no irAE) across CD8 T cells. (H) Pseudo-bulk analysis showing expression levels of 14 genes from (G). The color indicates expression levels of each gene among different prognosis groups. (I) Violin plot indicating overlapped 14 genes score between response and no response groups from public data (GSE216329). (J) Violin plot showing two biological pathways score between response and no response groups from public data. CD8 T-cell activation (left) and NK cell-mediated cytotoxicity (right). (K) Venn diagram showing the number of overlapping genes between 14 genes and genes differentially increased in the response group of public data. (L) Violin plot showing two candidate expressions between the three prognosis groups from CD8 T cells of no irAE samples. (M) Line plot demonstrating the correlation between CD8 T-cell activation score and whole genes in CD8 T cells. The two candidate genes we found in (K) are labeled on the plot. (N) Box plot illustrating changes in the proportion of cells with higher expression levels than an average expression of *PRF1* in CD8 T cells in the prognosis group (left) and irAE group (right). (O) Box plot illustrating the proportion of cells with higher expression levels than an average expression of *PRF1* in CD8 T cells in the response group (left) and irAE grade group (right) from public data (GSE216329). (P) Bee swarm plot indicating perforin expression levels among three irAE groups. The y-axis indicates expression levels. ∗p<0.05, ∗∗p<0.01, ∗∗∗p<0.001. (Q) Bar plot indicating proportion changes of cells showing higher expression levels than the mean (left) and median expression (right) of perforin among three prognosis groups from the CBA assay. (R) Bar plot indicating proportion changes of cells showing higher expression levels than the mean (left) and median expression (right) of perforin among three irAE groups from the CBA assay. AR, acquired resistance; CBA, cytometric bead array; CR, complete remission; DEG, differentially-expressed gene; irAE, immune-related adverse event; NK, natural killer; priR, primary resistance; TCR, T-cell receptor.

enriched in immune activation functions and were significantly upregulated in both the CR and mild/moderate irAE groups (figure 7D–F).

Among these 48 genes, 14 were specifically upregulated in the mild/moderate irAE group compared with the other subgroups, with significant involvement in NK-mediated cytotoxicity and CD8 T-cell activation, both supporting antitumor responses (figure 7G and H, (online supplemental figure S11B). These 14 genes were also upregulated in the immunotherapy response group of the public datasets, with the enrichment of two pathways associated with antitumor effects (figure 7I and J). Among the 14 genes, we identified *PRF1* and *RAP1GAP2* as being differentially upregulated in the public datasets (figure 7K). In particular, we focused on *PRF1*, which exhibited increased expression in both the CR and mild/moderate irAE within CD8 T cells and were significantly upregulated in the CR of no irAE samples (figure 7L and online supplementalfigure S11C, D). Additionally, *PRF1* strongly correlated with NK-mediated cytotoxicity and CD8 T-cell activation and was increased in almost all CD8 T-cell subtypes from CR and mild/moderate irAEs (figure 7M; online supplemental figure S11E, F). Patients with high *PRF1* expression in CD8 T cells were more frequently observed in the CR than in the AR or priR groups, with the highest proportion in the mild/moderate irAE subgroup compared with the no irAE and severe irAE groups (figure 7N). Interestingly, there were no significant proportional differences among groups within the different conditions, such as PD-L1 expression, tumor histology, and treatment regimen (online supplemental figure S11G). Further, *PRF1* was increased in almost all CD8 T-cell subtypes in the CR, irrespective of conditions such as PD-L1 expression levels, tumor histology, and treatment regimen (online supplemental figure S12A). Similarly, in the comparison between irAE groups, most CD8 T-cell subtypes were elevated in the mild/moderate irAE across all conditions, except for NSCLC NOS (histology) and N/A (regimen) (online supplemental figure S12B). The public data further supported the finding that patients with high *PRF1* expression in CD8 T cells were primarily found in the response and mild/moderate irAE groups (figure 7O). Perforin expression, validated using a CBA, showed a significant increase in mild/moderate irAE (figure 7P). Furthermore, we identified that patients with higher expression of perforin were majorly composed of CR and mild/moderate or no irAE using the CBA (figure 7Q, R). Similarly, granzyme B, which was CR specifically upregulated in the CD8 T and NK cells, increased in the no and mild/moderate irAE (online supplemental figure S13A, B). Additionally, we confirmed that its expression was elevated in the no irAE compared with severe irAE using CBA, and the patients showing higher expression of granzyme B were majorly distributed in the CR and no irAE groups (online supplemental figure S13C-E).

In summary, we have identified valuable biomarkers for predicting ICI efficacy and irAE severity in baseline PBMC. Our study sheds light on establishing appropriate guidelines for immunotherapy to enhance patient care and treatment outcomes.

DISCUSSION

In this study, we performed scRNA-seq of baseline PBMCs collected immediately before treatment from patients with lung cancer undergoing ICI treatment. We investigated the mechanisms underlying CR and distinguished them from those associated with priR and AR. In addition, we identified monocytes as a novel cell type strongly associated with the occurrence of irAEs. Based on these findings, we validated IL1B and CXCL8 as predictive markers of irAEs in a large cohort. In addition, we analyzed the overlapping pathways between mild-to-moderate irAEs and CR, driven by findings from multiple retrospective studies showing that patients experiencing mild-to-moderate irAEs tend to exhibit better treatment responses and improved prognoses.[32 33 50] To support and extend these findings, we conducted additional validation in a larger patient cohort, analyzing plasma levels of perforin, granzyme B, and IFN-γ. These factors were investigated for their potential utility as clinically applicable biomarkers predictive of both therapeutic response and irAEs.

ICI treatment offers a significant paradigm shift in the treatment of patients with advanced lung cancer as it has the potential to induce durable responses and, in some cases, achieve CR.[51 52] However, long-term follow-up data for pembrolizumab showed that the rate of patients maintaining a CR was approximately 1% in the entire cohort.[53] In this context, identifying the characteristic mechanisms associated with CR is crucial for overcoming ICI resistance. In our cohort, CD8 T cells were the most critical cells for achieving CR. Notably, the gene expression of granzyme and perforin in these cells showed significant differences compared with that of priR and AR, suggesting that the cytotoxic T-cell immune response plays a crucial role. This finding aligns with previously established knowledge,[54] and it has been reported that higher baseline concentrations of perforin are associated with longer progression-free survival and overall survival (OS) after ICI treatment.[55 56] Interestingly, while there was a clear distinction in the expression patterns between CR and those with priR or AR, priR and AR showed similar expression profiles. However, pathways related to hypoxia and the UV response were significantly more pronounced in priR than in AR. These findings suggest that hypoxia is associated with priR. Moreover, the inhibition of the TF HIF1A, a crucial regulator of hypoxia, overcomes resistance to PD-1 blockade, thereby enhancing the efficacy of ICIs.[57 58] Additionally, HIF1A inhibits interferon signaling, which is activated in CR.[59] Indeed, tumors associated with necrosis are often considered to be in a hypoxic environment, and there are reports indicating that such conditions are associated with a poor response to ICI treatment.[60 61]

In addition to CD8 T cells, CD4 T cells play a crucial role in regulating cytotoxic T-cell responses and in performing antitumor functions.[62] Notably, high expression levels of the guanylate-binding protein (GBP) family have emerged as predictive markers for positive immunotherapy responses, strongly correlating with improved OS outcomes.[63] Consistent with previous findings, our study revealed an increase in *GBP1* and *GBP2*, which were all positively associated with immune cell infiltration, leading to improved OS of ICIs, thus reinforcing their prognostic significance in the context of ICI therapy.[64–66] STAT1 also modulates various inflammatory cytokine signaling pathways, and signatures activated by STAT1 improve the prognosis of ICI.[67]

In addition, in NK cells from CR, high expression of *ITGAL*, *GZMB*, and *PRF1*, which are associated with targeting and are essential for the efficient maturation and antitumor of NK cells, was confirmed.[45] Previous lung cancer research revealed that ITGAL expression in NK cells was higher in normal tissues than in tumor samples, and that groups with high ITGAL expression demonstrated potential for improved immunotherapy outcomes.[68] This finding suggests the high utility of ITGAL-mediated NK cells in predicting ICI prognosis.

As the clinical application of ICIs expands across various cancer types and stages, clinicians increasingly encounter irAEs that can manifest in a wide range of organs and various forms.[69 70] These irAEs may become an obstacle to maintaining ICI treatment and, in severe cases, may require permanent discontinuation and may even threaten survival.[71 72] In particular, immune-related pneumonitis occurs more frequently in patients with lung cancer than in those with other carcinomas, requiring attention[73 74]; however, there is currently no marker that can predict the occurrence of irAEs. IrAEs occur because of the overactivation of the immune system induced by ICIs, which disrupts self-tolerance and fosters autoimmune reactions at various immunopathological levels.[75] This phenomenon is believed to result from various mechanisms, including the autoreactive effects of CD4 and CD8 T cells, the release of self-antigens from tumor cells, the activation of autoreactive B cells, and the abnormal release of proinflammatory mediators such as cytokines and chemokines, which drive to systemic inflammation.[76] Multiple studies have linked cytokines such as tumor necrosis factor (TNF)-alpha, interleukin (IL)-6, IL-17, IL-1β, and IL-10 to the development of irAEs.[77] Recent research has highlighted that an early increase in CXCL9, CXCL10, CXCL11, and IFN-γ within 1–2 weeks following therapy initiation may indicate a higher risk of irAEs. Additionally, early expansion of Ki-67+regulatory and Ki-67+CD8+ T cells has been associated with a higher risk of irAEs.[78] While most previous studies have linked irAEs primarily associated with T-cell subpopulations, our research identified that several immune response-related signaling pathways, including TNF-alpha signaling, are predominantly elevated in monocytes. One study reported that the CD16+monocyte population increased significantly in both mild and severe irAE cases, comprising a larger proportion of the total PBMC population compared with the cancer control group, whereas CD14+monocytes were more prevalent in irAE patients, with a notable increase observed in mild cases compared with severe cases.[79] This suggests that monocytes are important for the occurrence of irAEs. We also identified potential candidates based on genes with increased expression in monocytes, of which CXCL8 and IL1B were validated using pretreatment baseline plasma samples from 175 patients. Validation revealed that these markers were notably elevated in patients who experienced irAEs, particularly in those with severe irAEs. Consistent with these results, recent research has shown that IL1B high-expressing monocytes in PBMCs differentiate into macrophages following immunotherapy, leading to inflammatory arthritis (IA) in synovial fluid mononuclear cells.[80] Moreover, CXCL2 and CXCL8, which play roles in recruiting immune cells and activating inflammatory responses, are significantly elevated in irAE patient samples in previous studies.[80–83] Given the upregulation of IL1B, CXCL2, and CXCL8 in monocytes from the baseline of our findings, this implies that the cytokines responsible for IA were already elevated at baseline, ultimately inducing irAE. This suggests that these markers could potentially be used for predicting irAEs in patients by using anti-CXCL8 (IL-8) antibodies[84] could be explored as a therapeutic option for preventing irAEs. Additionally, considering that EREG and CCL3 expression is increased in IL1B-high monocytes, which are closely associated with irAE-IA and irAE-pneumonitis, that these molecules are actively involved in proinflammatory activities, EREG and CCL3 may suggest a close relationship between these molecules and irAEs.[80 83 85 86]

Numerous studies have investigated the association between irAEs and effectiveness of ICIs, particularly in NSCLC.[50] In pooled analyses of the IMpower trials, patients with irAEs, particularly grades 1–2, showed significantly longer OS compared with those without irAEs.[87] Similarly, other studies reported that irAEs, especially endocrine-related events such as thyroid dysfunction, are associated with improved objective response rates, progression-free survival, and OS.[88] Notably, patients experiencing multisystem irAEs demonstrated even greater survival benefits than those experiencing single or no irAEs.[89] However, this relationship is complex and influenced by various factors such as the type, severity, timing of onset, and management of irAEs, all of which can affect treatment outcomes. Moreover, confounding variables should be considered when assessing the association between irAEs and survival rates. For example, patients with longer survival duration may be more likely to develop irAEs because of extended exposure to ICIs. Consequently, the usefulness of irAEs as reliable surrogate markers of ICI efficacy remains unclear. Furthermore, the underlying mechanisms linking irAEs to improved treatment efficacy and prognosis remain unclear and require further investigation. In this study, we identified specific pathways shared between mild-to-moderate irAEs and ICI efficacy,

providing novel insights into the potential biological basis of this association. NK-mediated cytotoxicity and CD8 T-cell activation pathways are commonly implicated in mild-to-moderate irAEs and improved efficacy. We validated these findings using a public dataset and found that *PRF1* was strongly associated with these pathways. This suggests that targeting PRF1 could enhance the efficacy of ICI treatment, potentially maximizing therapeutic outcomes. However, appropriate biomarkers predicting ICI response and irAE severity are still not established, and there are challenges in selecting candidates beforehand. In our analysis, we found that higher baseline plasma levels of perforin and granzyme B were significantly associated with both favorable treatment response and a lower incidence of severe irAEs. These observations suggest the potential clinical utility of these cytotoxic effector molecules as non-invasive biomarkers for patient stratification prior to ICI therapy. Pretreatment assessment of perforin and granzyme B levels may aid in identifying patients more likely to derive clinical benefit while minimizing the risk of severe toxicity.

This study has several limitations. First, patients with intermediate response patterns—such as initial stable disease or partial response followed by early progression within 6 months—were not included. Future studies including these subgroups are needed to better reflect real-world clinical heterogeneity. Second, while peripheral blood samples are more suitable for biomarker discovery, their profiles may not fully represent the tumor microenvironment. In advanced lung cancer, limited tissue availability from small biopsies makes direct comparison challenging. Integrating data from both peripheral blood and tumor tissue, when available, would provide a more comprehensive understanding of immunotherapy responses.

Our study focused on pretreated PBMC samples to present biomarkers to select appropriate patients likely to have a good prognosis and low irAEs before ICI treatment. However, longitudinal analyses can show how changes in these biomarkers influence ICI prognosis and irAE. Furthermore, by tracking gradual gene expression and cell type variations, we may identify new biomarkers that can estimate disease progression and irAE severity from each stage, providing insights for tracking the ICI effectiveness and treatment optimization. Although we focused on pretreated samples in this study, we increased the practical applicability of these biomarkers by validating them using larger cohorts and public datasets. In addition to predicting treatment outcomes, these biomarkers have been used as targets to enhance or mitigate treatment responsiveness and irAEs. Collectively, our work highlights the potential of establishing and improving ICI treatment strategies before treatment using PBMC samples.

Contributors GDK, DHK and JP performed study concept and design. DHK and JP supervised the project. S-IS constructed TCR sequencing library. PS, JEL, CC, YEK and DHK collected the patient samples and clinical characteristics. DHK performed a cytometric bead array. GDK analyzed the single-cell data. GDK, DHK and JP wrote the manuscript and all authors revised the manuscript with supportive advice. The authors read and approved the final manuscript. JP and DHK are the guarantors.

Funding This work was supported GIST-CNUH Research Collaboration grant and GIST-MIT Research collaboration grant funded by the GIST in 2024; the National Research Foundation of Korea (NRF), funded by the Korean government (RS-2024-00335026, RS-2024-00403622, RS-2019-NR040068, RS-2022-NR071878). This research was supported by a grant from the Korea Health Technology R&D Project through the Korea Health Industry Development Institute (KHIDI), funded by the Ministry of Health & Welfare, Republic of Korea (RS-2022-KH130308).

Competing interests No, there are no competing interests.

Patient consent for publication Not applicable.

Ethics approval The study adhered to the Declaration of Helsinki and Good Clinical Practice guidelines and secured approval from the institutional review board of each participating institution (2018-04-014 at Chungnam National University Hospital). Written informed consent was obtained from all patients prior to their inclusion in the study.

Provenance and peer review Not commissioned; externally peer reviewed.

Data availability statement Data are available in a public, open access repository. Data are available upon reasonable request. The processed data in this study are publicly available in Gene Expression Omnibus (GEO) at GSE285888. All other raw data generated in this study are available upon request from the corresponding author.

ORCID iDs
Gyeong Dae Kim http://orcid.org/0000-0002-9288-6341
Da Hyun Kang http://orcid.org/0000-0002-3495-0931

REFERENCES

1 Lim SM, Hong MH, Kim HR. Immunotherapy for Non-small Cell Lung Cancer: Current Landscape and Future Perspectives. *Immune Netw* 2020;20:e10.
2 Shukla N, Hanna N. Neoadjuvant and Adjuvant Immunotherapy in Early-Stage Non-Small Cell Lung Cancer. *Lung Cancer (Auckl)* 2021;12:51–60.
3 Carbone DP, Gandara DR, Antonia SJ, *et al*. Non-Small-Cell Lung Cancer: Role of the Immune System and Potential for Immunotherapy. *J Thorac Oncol* 2015;10:974–84.
4 Sharma P, Hu-Lieskovan S, Wargo JA, *et al*. Primary, Adaptive, and Acquired Resistance to Cancer Immunotherapy. *Cell* 2017;168:707–23.
5 Zhou S, Yang H. Immunotherapy resistance in non-small-cell lung cancer: From mechanism to clinical strategies. *Front Immunol* 2023;14:1129465.
6 Memon D, Hellmann M, Miller M. 522 Clinical and molecular features of acquired resistance to immunotherapy in non-small cell lung cancer. SITC 37th Annual Meeting (SITC 2022) Abstracts; 2022
7 Sun Q, Wei X, Wang Z, *et al*. Primary and Acquired Resistance against Immune Check Inhibitors in Non-Small Cell Lung Cancer. *Cancers (Basel)* 2022;14:3294.
8 Francisco LM, Sage PT, Sharpe AH. The PD-1 pathway in tolerance and autoimmunity. *Immunol Rev* 2010;236:219–42.
9 Jhaveri KD, Perazella MA. Adverse Events Associated with Immune Checkpoint Blockade. *N Engl J Med* 2018;378:1163.

10 Postow MA, Sidlow R, Hellmann MD. Immune-Related Adverse Events Associated with Immune Checkpoint Blockade. *N Engl J Med* 2018;378:158–68.
11 Pillai RN, Behera M, Owonikoko TK, *et al*. Comparison of the toxicity profile of PD-1 versus PD-L1 inhibitors in non-small cell lung cancer: A systematic analysis of the literature. *Cancer* 2018;124:271–7.
12 Kim KH, Hur JY, Cho J, *et al*. Immune-related adverse events are clustered into distinct subtypes by T-cell profiling before and early after anti-PD-1 treatment. *Oncoimmunology* 2020;9:1722023.
13 Wang DY, Salem J-E, Cohen JV, *et al*. Fatal Toxic Effects Associated With Immune Checkpoint Inhibitors: A Systematic Review and Meta-analysis. *JAMA Oncol* 2018;4:1721–8.
14 Luo H, Xia X, Kim GD, *et al*. Characterizing dedifferentiation of thyroid cancer by integrated analysis. *Sci Adv* 2021;7:eabf3657.
15 Li P-H, Kong X-Y, He Y-Z, *et al*. Recent developments in application of single-cell RNA sequencing in the tumour immune microenvironment and cancer therapy. *Mil Med Res* 2022;9:52.
16 Luo H, Xia X, Huang L-B, *et al*. Pan-cancer single-cell analysis reveals the heterogeneity and plasticity of cancer-associated fibroblasts in the tumor microenvironment. *Nat Commun* 2022;13:6619.
17 Fleming SJ, Chaffin MD, Arduini A, *et al*. Unsupervised removal of systematic background noise from droplet-based single-cell experiments using CellBender. *Nat Methods* 2023;20:1323–35.
18 Kim GD, Shin S-I, Jung SW, *et al*. Cell Type– and Age-Specific Expression of lncRNAs across Kidney Cell Types. *JASN* 2024;35:870–85.
19 Kim GD, Lim C, Park J. A practical handbook on single-cell RNA sequencing data quality control and downstream analysis. *Mol Cells* 2024;47:100103.
20 McGinnis CS, Murrow LM, Gartner ZJ. DoubletFinder: Doublet Detection in Single-Cell RNA Sequencing Data Using Artificial Nearest Neighbors. *Cell Syst* 2019;8:329–37.
21 Hao Y, Hao S, Andersen-Nissen E, *et al*. Integrated analysis of multimodal single-cell data. *Cell* 2021;184:3573–87.
22 Korsunsky I, Millard N, Fan J, *et al*. Fast, sensitive and accurate integration of single-cell data with Harmony. *Nat Methods* 2019;16:1289–96.
23 Bolotin DA, Poslavsky S, Mitrophanov I, *et al*. MiXCR: software for comprehensive adaptive immunity profiling. *Nat Methods* 2015;12:380–1.
24 Fiadziushchanka S, Rumynskiy E, Popov A, *et al*. Bioinformatics analysis of t-cell and b-cell immune repertoires. 2023. Available: https://immunarch.com/, https://github.com/immunomind/immunarch
25 Efremova M, Vento-Tormo M, Teichmann SA, *et al*. CellPhoneDB: inferring cell-cell communication from combined expression of multi-subunit ligand-receptor complexes. *Nat Protoc* 2020;15:1484–506.
26 Browaeys R, Saelens W, Saeys Y. NicheNet: modeling intercellular communication by linking ligands to target genes. *Nat Methods* 2020;17:159–62.
27 Morabito S, Reese F, Rahimzadeh N, *et al*. hdWGCNA identifies co-expression networks in high-dimensional transcriptomics data. *Cell Rep Methods* 2023;3:100498.
28 Liberzon A, Birger C, Thorvaldsdóttir H, *et al*. The Molecular Signatures Database (MSigDB) hallmark gene set collection. *Cell Syst* 2015;1:417–25.
29 Kanehisa M, Furumichi M, Tanabe M, *et al*. KEGG: new perspectives on genomes, pathways, diseases and drugs. *Nucleic Acids Res* 2017;45:D353–61.
30 Kuleshov MV, Jones MR, Rouillard AD, *et al*. Enrichr: a comprehensive gene set enrichment analysis web server 2016 update. *Nucleic Acids Res* 2016;44:W90–7.
31 Huang DW, Sherman BT, Tan Q, *et al*. The DAVID Gene Functional Classification Tool: a novel biological module-centric algorithm to functionally analyze large gene lists. *Genome Biol* 2007;8:R183.
32 Wang W, Gu X, Wang L, *et al*. The prognostic impact of mild and severe immune-related adverse events in non-small cell lung cancer treated with immune checkpoint inhibitors: a multicenter retrospective study. *Cancer Immunol Immunother* 2022;71:1693–703.
33 Haratani K, Hayashi H, Chiba Y, *et al*. Association of Immune-Related Adverse Events With Nivolumab Efficacy in Non-Small-Cell Lung Cancer. *JAMA Oncol* 2018;4:374–8.
34 Noman MZ, Hasmim M, Messai Y, *et al*. Hypoxia: a key player in antitumor immune response. A Review in the Theme: Cellular Responses to Hypoxia. *Am J Physiol Cell Physiol* 2015;309:C569–79.
35 Katiyar SK. UV-induced immune suppression and photocarcinogenesis: chemoprevention by dietary botanical agents. *Cancer Lett* 2007;255:1–11.
36 Ziello JE, Jovin IS, Huang Y. Hypoxia-Inducible Factor (HIF)-1 regulatory pathway and its potential for therapeutic intervention in malignancy and ischemia. *Yale J Biol Med* 2007;80:51–60.
37 Tian H, Hammer RE, Matsumoto AM, *et al*. The hypoxia-responsive transcription factor EPAS1 is essential for catecholamine homeostasis and protection against heart failure during embryonic development. *Genes Dev* 1998;12:3320–4.
38 Samarin J, Wessel J, Cicha I, *et al*. FoxO proteins mediate hypoxic induction of connective tissue growth factor in endothelial cells. *J Biol Chem* 2010;285:4328–36.
39 Triner D, Shah YM. Hypoxia-inducible factors: a central link between inflammation and cancer. *J Clin Invest* 2016;126:84430:3689–98:.
40 Bukhari S, Henick BS, Winchester RJ, *et al*. Single-cell RNA sequencing reveals distinct T cell populations in immune-related adverse events of checkpoint inhibitors. *Cell Rep Med* 2023;4:100868.
41 Hoves S, Sutton VR, Trapani JA. A novel role for granzymes in anti-tumor immunity. *Oncoimmunology* 2012;1:219–21.
42 Stewart SE, Kondos SC, Matthews AY, *et al*. The Perforin Pore Facilitates the Delivery of Cationic Cargos. *Journal of Biological Chemistry* 2014;289:9172–81.
43 Lelliott EJ, Ramsbottom KM, Dowling MR, *et al*. NKG7 Enhances CD8+ T Cell Synapse Efficiency to Limit Inflammation. *Front Immunol* 2022;13:931630.
44 Erokhina SA, Streltsova MA, Kanevskiy LM, *et al*. HLA-DR-expressing NK cells: Effective killers suspected for antigen presentation. *J Leukoc Biol* 2021;109:327–37.
45 Urlaub D, Höfer K, Müller M-L, *et al*. LFA-1 Activation in NK Cells and Their Subsets: Influence of Receptors, Maturation, and Cytokine Stimulation. *J Immunol* 2017;198:1944–51.
46 Zhang Z, Zhang Y, Xia S, *et al*. Gasdermin E suppresses tumour growth by activating anti-tumour immunity. *Nature New Biol* 2020;579:415–20.
47 Prager I, Liesche C, van Ooijen H, *et al*. NK cells switch from granzyme B to death receptor-mediated cytotoxicity during serial killing. *J Exp Med* 2019;216:2113–27.
48 Taylor CT, Colgan SP. Regulation of immunity and inflammation by hypoxia in immunological niches. *Nat Rev Immunol* 2017;17:774–85.
49 Hu W-T, Zhang Q, Zhang Z, *et al*. Eosinophil and IFN-γ associated with immune-related adverse events as prognostic markers in patients with non-small cell lung cancer treated with immunotherapy. *Front Immunol* 2023;14:1112409.
50 Fukushima T, Kobayashi S, Ueno M. The correlation between immune-related adverse events and efficacy of immune checkpoint inhibitors. *Jpn J Clin Oncol* 2024;54:949–58.
51 Reck M, Rodríguez-Abreu D, Robinson AG, *et al*. Five-Year Outcomes With Pembrolizumab Versus Chemotherapy for Metastatic Non-Small-Cell Lung Cancer With PD-L1 Tumor Proportion Score ≥ 50. *J Clin Oncol* 2021;39:2339–49.
52 Shalata W, Zolnoorian J, Migliozzi G, *et al*. Long-Lasting Therapeutic Response following Treatment with Pembrolizumab in Patients with Non-Small Cell Lung Cancer: A Real-World Experience. *Int J Mol Sci* 2023;24:5938.
53 de Castro G Jr, Kudaba I, Wu Y-L, *et al*. Five-Year Outcomes With Pembrolizumab Versus Chemotherapy as First-Line Therapy in Patients With Non–Small-Cell Lung Cancer and Programmed Death Ligand-1 Tumor Proportion Score ≥ 1% in the KEYNOTE-042 Study. *JCO* 2023;41:1986–91.
54 Durgeau A, Virk Y, Corgnac S, *et al*. Recent Advances in Targeting CD8 T-Cell Immunity for More Effective Cancer Immunotherapy. *Front Immunol* 2018;9:14.
55 Ota T, Fukui T, Nakahara Y, *et al*. Serum immune modulators during the first cycle of anti-PD-1 antibody therapy in non-small cell lung cancer: Perforin as a biomarker. *Thorac Cancer* 2020;11:3223–33.
56 Chung JH, Ha JS, Choi J, *et al*. Granzyme B for predicting the durable clinical benefit of anti-PD-1/PD-L1 immunotherapy in patients with non-small cell lung cancer. *Transl Cancer Res* 2022;11:316–26.
57 Ma S, Zhao Y, Lee WC, *et al*. Hypoxia induces HIF1α-dependent epigenetic vulnerability in triple negative breast cancer to confer immune effector dysfunction and resistance to anti-PD-1 immunotherapy. *Nat Commun* 2022;13:4118.
58 Luo F, Lu F-T, Cao J-X, *et al*. HIF-1α inhibition promotes the efficacy of immune checkpoint blockade in the treatment of non-small cell lung cancer. *Cancer Lett* 2022;531:39–56.
59 Peng T, Du S-Y, Son M, *et al*. HIF-1α is a negative regulator of interferon regulatory factors: Implications for interferon production by hypoxic monocytes. *Proc Natl Acad Sci USA* 2021;118.
60 Lu T, Zhang L, Chen M, *et al*. Intrapulmonic Cavity or Necrosis on Baseline CT Scan Serves as an Efficacy Predictor of Anti-PD-(L)1

Inhibitor in Advanced Lung Squamous Cell Carcinoma. *Cancer Manag Res* 2021;13:5931–9.
61 Mortezaee K, Majidpoor J, Kharazinejad E. The impact of hypoxia on tumor-mediated bypassing anti-PD-(L)1 therapy. *Biomedicine & Pharmacotherapy* 2023;162:114646.
62 Ben Khelil M, Godet Y, Abdeljaoued S, *et al*. Harnessing Antitumor CD4+ T Cells for Cancer Immunotherapy. *Cancers (Basel)* 2022;14:260.
63 Ning Y, Fang S, Fang J, *et al*. Guanylate-binding proteins signature predicts favorable prognosis, immune-hot microenvironment, and immunotherapy response in hepatocellular carcinoma. *Cancer Med* 2023;12:17504–21.
64 Zhao Y, Wu J, Li L, *et al*. Guanylate-Binding Protein 1 as a Potential Predictor of Immunotherapy: A Pan-Cancer Analysis. *Front Genet* 2022;13.
65 Wang Y, Pan J, An F, *et al*. GBP2 is a prognostic biomarker and associated with immunotherapeutic responses in gastric cancer. *BMC Cancer* 2023;23:925.
66 Zhou W, Yeerkenbieke G, Zhang Y, *et al*. Guanylate binding protein 4 shapes an inflamed tumor microenvironment and identifies immuno-hot tumors. *J Cancer Res Clin Oncol* 2024;150:90.
67 Zemek RM, De Jong E, Chin WL, *et al*. Sensitization to immune checkpoint blockade through activation of a STAT1/NK axis in the tumor microenvironment. *Sci Transl Med* 2019;11:eaav7816.
68 Xiao Z, Nian Z, Zhang M, *et al*. Integrated analysis highlights the significance role of ITGAL in lung adenocarcinoma. *J Cell Mol Med* 2024;28:e18289.
69 Ramos-Casals M, Brahmer JR, Callahan MK, *et al*. Immune-related adverse events of checkpoint inhibitors. *Nat Rev Dis Primers* 2020;6:38.
70 Thompson JA, Schneider BJ, Brahmer J, *et al*. Management of Immunotherapy-Related Toxicities, Version 1.2022, NCCN Clinical Practice Guidelines in Oncology. *J Natl Compr Canc Netw* 2022;20:387–405.
71 Russano M, Cortellini A, Giusti R, *et al*. Clinical outcomes of NSCLC patients experiencing early immune-related adverse events to PD-1/PD-L1 checkpoint inhibitors leading to treatment discontinuation. *Cancer Immunol Immunother* 2022;71:865–74.
72 Ruste V, Goldschmidt V, Laparra A, *et al*. The determinants of very severe immune-related adverse events associated with immune checkpoint inhibitors: A prospective study of the French REISAMIC registry. *Eur J Cancer* 2021;158:217–24.
73 Chen X, Zhang Z, Hou X, *et al*. Immune-related pneumonitis associated with immune checkpoint inhibitors in lung cancer: a network meta-analysis. *J Immunother Cancer* 2020;8:e001170.
74 Tiu BC, Zubiri L, Iheke J, *et al*. Real-world incidence and impact of pneumonitis in patients with lung cancer treated with immune checkpoint inhibitors: a multi-institutional cohort study. *J Immunother Cancer* 2022;10:e004670.
75 Esfahani K, Elkrief A, Calabrese C, *et al*. Moving towards personalized treatments of immune-related adverse events. *Nat Rev Clin Oncol* 2020;17:504–15.
76 Casagrande S, Sopetto GB, Bertalot G, *et al*. Immune-Related Adverse Events Due to Cancer Immunotherapy: Immune Mechanisms and Clinical Manifestations. *Cancers (Basel)* 2024;16:1440.
77 Les I, Martínez M, Pérez-Francisco I, *et al*. Predictive Biomarkers for Checkpoint Inhibitor Immune-Related Adverse Events. *Cancers (Basel)* 2023;15:1629.
78 Nuñez NG, Berner F, Friebel E, *et al*. Immune signatures predict development of autoimmune toxicity in patients with cancer treated with immune checkpoint inhibitors. *Med* 2023;4:113–29.
79 Garrison Z, Chang M, Hornick N, *et al*. A Novel Potential Role for Monocytes Revealed by Single Cell Analysis of Immunotherapy Induced Immune Related Adverse Events. *Cancers (Basel)* 2022;14:5407.
80 Zhou Z, Zhou X, Jiang X, *et al*. Single-cell profiling identifies IL1Bhi macrophages associated with inflammation in PD-1 inhibitor-induced inflammatory arthritis. *Nat Commun* 2024;15:2107.
81 Ha H, Debnath B, Neamati N. Role of the CXCL8-CXCR1/2 Axis in Cancer and Inflammatory Diseases. *Theranostics* 2017;7:1543–88.
82 Khan S, Khan SA, Luo X, *et al*. Immune dysregulation in cancer patients developing immune-related adverse events. *Br J Cancer* 2019;120:63–8.
83 Franken A, Van Mol P, Vanmassenhove S, *et al*. Single-cell transcriptomics identifies pathogenic T-helper 17.1 cells and pro-inflammatory monocytes in immune checkpoint inhibitor-related pneumonitis. *J Immunother Cancer* 2022;10:e005323.
84 Huang S, Mills L, Mian B, *et al*. Fully humanized neutralizing antibodies to interleukin-8 (ABX-IL8) inhibit angiogenesis, tumor growth, and metastasis of human melanoma. *Am J Pathol* 2002;161:125–34.
85 Harada M, Kamimura D, Arima Y, *et al*. Temporal expression of growth factors triggered by epiregulin regulates inflammation development. *J Immunol* 2015;194:1039–46.
86 Baba T, Mukaida N. Role of macrophage inflammatory protein (MIP)-1α/CCL3 in leukemogenesis. *Mol Cell Oncol* 2014;1:e29899.
87 Socinski MA, Jotte RM, Cappuzzo F, *et al*. Association of Immune-Related Adverse Events With Efficacy of Atezolizumab in Patients With Non-Small Cell Lung Cancer: Pooled Analyses of the Phase 3 IMpower130, IMpower132, and IMpower150 Randomized Clinical Trials. *JAMA Oncol* 2023;9:527–35.
88 Grangeon M, Tomasini P, Chaleat S, *et al*. Association Between Immune-related Adverse Events and Efficacy of Immune Checkpoint Inhibitors in Non-small-cell Lung Cancer. *Clin Lung Cancer* 2019;20:201–7.
89 Shankar B, Zhang J, Naqash AR, *et al*. Multisystem Immune-Related Adverse Events Associated With Immune Checkpoint Inhibitors for Treatment of Non-Small Cell Lung Cancer. *JAMA Oncol* 2020;6:1952–6.